Lawrence Berkeley Laboratory
UNIVERSITY OF CALIFORNIA

Materials & Molecular Research Division

Submitted to the Journal of the Electrochemical Society

THERMODYNAMICS OF LOW-TEMPERATURE (700-850°C) HOT CORROSION

A.K. Misra, D.P. Whittle, and W.L. Worrell

September 1980

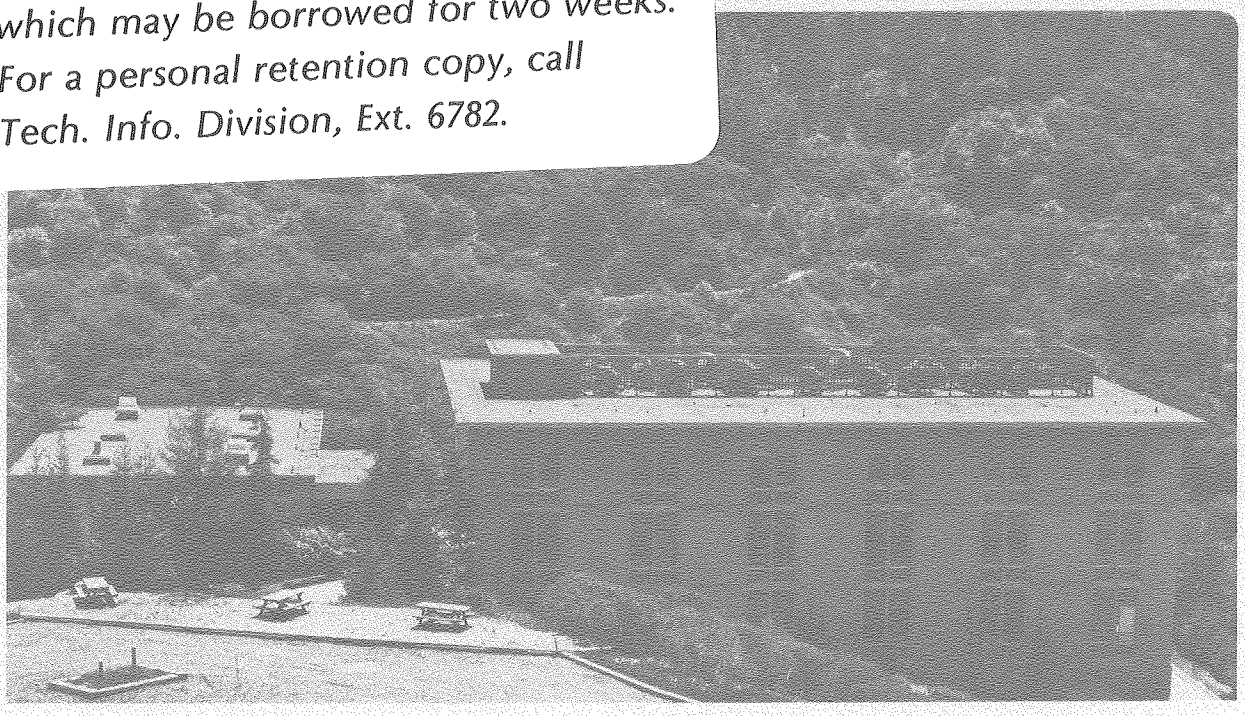

Prepared for the U.S. Department of Energy under Contract W-7405-ENG-48

DISCLAIMER

LBL-11495

THERMODYNAMICS OF LOW-TEMPERATURE (700-850°C) HOT CORROSION

A.K. Misra and D.P. Whittle*
Lawrence Berkeley Laboratory
and
Materials Science and Mineral Engineering
University of California
Berkeley CA 94720

W.L. Worrell*
Department of Metallurgy
University of Pennsylvania
Philadelphia PA

Abstract

Existing phase diagrams in the systems Na_2SO_4 - MSO_4 (M=Ni,Co) and Na_2SO_4 - $M_2(SO_4)_3$ (M=Al,Fe,Cr) have been used to calculate the thermodynamic properties of the molten sulfate systems. The calculated thermodynamic data show satisfactory agreement with most of the available experimental observations. The calculations have shown that the activity of $Al_2(SO_4)_3$ and $Fe_2(SO_4)_3$ in the melt can be lowered to such an extent that liquid sulfate solutions can be formed at P_{SO_3} levels that are prevalent in marine gas turbine operations, and this has been explained on the basis of complex formation in the melt. Thermodynamic analysis of the interaction of the Na_2SO_4 - MSO_4 (M=Co,Ni) melt with protective oxides Al_2O_3 and Cr_2O_3 has demonstrated the vulnerability of Al-containing alloys to hot corrosion attack.

---

*Electrochemical Society Active Member

Key words: hot corrosion, thermodynamics, sulfates, nickel, cobalt.

1. Introduction

The low-temperature (650-850°C) corrosion of blades and first-stage guide vanes of gas turbines exposed to marine and industrial atmospheres has received considerable attention in the recent past. The corrosion is primarily due to a deposit of Na_2SO_4 on the blade surface and, depending on the temperature, the deposit is either molten or solid. Although the corrosion mechanism in the temperature range 650-850°C, where the Na_2SO_4 deposit is solid, is still being debated, there appears to be a general consensus among several workers (1,2,3) that favors the formation of molten mixed sulfates, (Na_2SO_4-MSO_4) (M = Co or Ni) or Na_2SO_4 - $M_2(SO_4)_3$ (M = Fe,Al,Cr), by the reaction of metal oxides with SO_2/SO_3 in the gas turbine atmosphere. The sulfur comes from impurities in the fuel. In contrast to hot corrosion above 900°C, where Na_2SO_4 is molten and the corrosion proceeds by interaction of metal oxides with Na_2SO_4 melt, the low-temperature (650-850°C) corrosion requires the formation of a liquid salt melt, which can then further interact with the metal or metal oxides. Thus, the low-temperature corrosion process can be divided into two stages: 1) formation of molten mixed sulfates, and 2) interaction of the molten salt mixture with the oxides of the alloying elements. The present study is concerned with both the formation of mixed sulfates and their interaction with the oxides of alloying elements.

The formation of a molten sulfate mixture depends on the SO_2/SO_3 level in the gas turbine atmosphere, and there is considerable controversy regarding a minimum threshold SO_2/SO_3 concentration in the atmosphere, below which corrosion will not occur. The formation of mixed sulfates can be described by the general reaction

$$M + SO_3 = MSO_4 \text{ (dissolved in } Na_2SO_4) \tag{1}$$

$$K_1 = \frac{a_{MSO_4}(\text{in melt})}{p_{SO_3}} \tag{2}$$

where K_1 is the equilibrium constant for reaction (1) and a_{MSO_4} is the activity of metal sulfate in the melt. The p_{SO_3} required for mixed sulfate formation will depend on the activity of the MSO_4 in the melt. In addition, a knowledge of the activities, and other partial molar properties, of various metal sulfates and other compounds in the molten sulfate mixture is essential to understand the interaction of the salt melt with different oxides. In spite of the considerable progress made in the field of molten salt chemistry (in particular, halide, nitride, and carbonate mixtures), the salt chemistry and thermodynamics of molten salt mixtures of alkali sulfates with other metal sulfates is poorly understood and few relevant data exist at present.

In view of this dearth of free energy and activity data for molten salt solutions, it is necessary to extract as much information as possible from the phase diagrams that are available. For the alkali-halide/metal-halide mixtures, there has been close agreement between the experimentally measured activities and those calculated from the phase diagrams (4). Fortunately, phase diagrams exist for most of the alkali-sulfate/metal-sulfate binaries (Na_2SO_4-$CoSO_4$, Na_2SO_4-$NiSO_4$, etc.), which are of importance in the low-temperature corrosion process. The present paper seeks to predict the thermodynamic properties, as well as the salt chemistry of the molten sulfate mixtures that are of importance in the hot corrosion process, using the relevant phase diagrams. The systems evaluated are

(1) Na_2SO_4 - $CoSO_4$,

(2) Na_2SO_4 - $NiSO_4$,

(3) Na_2SO_4 - $Fe_2(SO_4)_3$,

(4) Na_2SO_4 - $Al_2(SO_4)_3$,

(5) Na_2SO_4 - $Cr_2(SO_4)_3$.

2. Theoretical Basis

2.1 Prediction of activities of the components in the melt

The depression of the freezing point of one salt brought about by the addition of another gives useful information about the activity of the solvent, and can be represented by the following equations, assuming a constant ΔH°_f (enthalpy of fusion)

Case (a): Liquid solution in equilibrium with pure solid:

$$\ln a_{solvent}(l) = \frac{\Delta H^{\circ}_{f}(T-T_m)}{RTT_m} \tag{3}$$

Case (b): Liquid solution in equilibrium with a solid solution, e.g., phase diagrams with a terminal solid solution:

$$\ln \frac{a_{solvent}(l)}{a_{solvent}(s)} = \frac{\Delta H^{\circ}_{f}(T-T_m)}{RTT_m} \tag{4}$$

where T and T_m are the temperature and melting point (K) of the solvent, respectively, ΔH°_{f} is the enthalpy of fusion and (l) and (s) refer to liquid and solid phases, respectively. In order to predict the activity of the solute, a regular solution model is frequently used (4), according to which

$$\begin{aligned} \ln \gamma_{solvent} &= \frac{\omega}{RT}(1 - x_{solvent})^2 \\ \ln \gamma_{solute} &= \frac{\omega}{RT}(1 - x_{solute})^2 \end{aligned} \tag{5}$$

where γ is the activity coefficient, x the mole fraction, and ω the interaction energy parameter for the solution. For the phase diagrams having a terminal solid solution, prediction of the activities of the components in the liquid mixture is further

complicated by the presence of the $a_{solvent}(s)$ term in Eq. (4). Two different approximations can be made to determine $a_{solvent}(s)$:

(1) An ideal solution behavior can be assumed in the solid state. However, the charge differences between the cations, which results in the formation of cation vacancies in the solvent sublattice, and size differences between cations, introduce large deviations from ideality, even at very low concentrations of the solute.

(2) A regular solution model can be assumed for the solid and, based on the assumption of temperature and concentration independence of the interaction energy parameter (ω), Eq. (4) can be written as

$$\ln\left(\frac{x_{solvent}(l)}{x_{solvent}(s)}\right) + \frac{\omega_L}{RT}(1-x_{solvent}(l))^2 - \frac{\omega_S}{RT}(1-x_{solvent}(s))^2 = \frac{\Delta H^\circ_f (T-T_m)}{RTT_m} \qquad (7)$$

The two unknowns ω_S and ω_L can be obtained by simultaneous solution of Eq. (7) for various solidus and liquidus compositions on the phase diagram at different temperatures. From the analysis of the phase diagrams, it was subsequently observed that any estimate of ω_L is insensitive to the values of ω_S, and so it was decided to assume the ideal solid solution behavior for all the systems.

2.2. Complex formation in the salt melt

From the activity data obtained by making use of the phase diagrams, useful information can also be obtained about the interaction between the solute and the solvent. Large negative deviations from ideality, which also involve large negative heats of mixing, would indicate a strong attractive interaction between the solute and the solvent that could lead to formation of complexes in the melt. If the interaction energy is large compared to thermal energy, complex formation is possible (5).

2.3. Thermodynamics of solutions involving complex ions

Consider a binary solution of A and B and let a complex A_iB_j be formed by reaction of i moles of A and j moles of B. If n_A and n_B are the initial number of moles of A and B, respectively, and n_A' and n_B' are the number of moles of A and B monomers respectively present in the solution after complex formation, then from mass balance considerations

$$n_A = n_A' + \sum_i \sum_j i n_{A_iB_j} \tag{8}$$

where $n_{A_iB_j}$ is the number of moles of the complex, and the summation is over all the different kind of complexes.

Similarly

$$n_B = n_B' + \sum_i \sum_j j n_{A_iB_j} \tag{9}$$

It can be shown that the chemical potentials μ_A and μ_B are equal to the chemical potentials of the respective monomers after complex formation. At equilibrium, if the solution is regarded as consisting of monomers of A and B and the complexes, all interaction between A and B that are strong enough to lead to complex formation are excluded. In the absence of any interaction between the monomer molecules and the complex, the solution can be approximated as an ideal solution, and thus we obtain

$$\mu_A = \mu_A' = \mu_A^\circ + RT \ln x_A' \tag{10}$$

$$\mu_B = \mu_B' = \mu_B^\circ + RT \ln x_B' \tag{11}$$

$$a_A = x_A' = \frac{n_A'}{n_A' + n_B' + \sum_i \sum_j n_{A_i B_j}} \tag{12}$$

$$a_B = x_B' = \frac{n_B'}{n_A' + n_B' + \sum_i \sum_j n_{A_i B_j}} \tag{13}$$

By the redefinition of the components in the melt, and by the careful choice of different complexes, the activities obtained from Eqs. (12) and (13) can be correlated with the activities derived from the phase diagrams, to give information on the complex species involved at equilibrium.

3. Na_2SO_4 - $CoSO_4$ System

The Na_2SO_4 - $CoSO_4$ phase diagram (6) is shown in Fig. 1. Only the Na_2SO_4-rich portion of the diagram (<48.6 mole percent $CoSO_4$) is taken for detailed analysis. Assuming an ideal solid solution behavior, the estimate of ω_L for the salt melt at various temperatures can be obtained from Eq. (7) (assuming $\omega_S = 0$) and is shown in Table I. The calculated ω_L values, assuming an ideal solid solution behavior, are fairly close to each other at all temperatures, and in the absence of any other available information about the thermodynamic properties of the system, the assumption of a temperature and concentration independent interaction energy parameter for the salt melt seems to be justified. An average value of $\omega_L = -7 \pm 1$ Kcal/mole can be estimated from Table I.

Now taking the estimated value of ω(-7 Kcal/mole) and assuming an ideal solid-solution behavior, the liquidus composition can be calculated and compared with the original phase diagram. The liquidus composition can be obtained by solving the following algebraic equation:

$$\ln x^{(l)}_{Na_2SO_4} = \frac{\omega_L}{RT}\left(1-x^{(l)}_{Na_2SO_4}\right)^2 - \ln x_{Na_2SO_4}(s) - \frac{\Delta H_f^{\circ}(T-Tm)}{RTTm} = 0 \qquad (14)$$

A comparison of the calculated liquidus compositions with those obtained from the phase diagram is shown in Table II. There is close agreement between the two different sets of values.

3.1. Verification of the interaction energy parameter (ω_L) from experimental data

Gupta and Rapp (7) have measured the solubility of Co_3O_4 in molten Na_2SO_4 at 1200°K, at different Na_2O activities (shown in Fig. 2). From their data in the acidic regime, in which Co_3O_4 dissolves as $CoSO_4$, a verificaton of the calculated interaction energy can be made. The dissolution of Co_3O_4 in molten Na_2SO_4 in the acidic regime can be described by the equilibrium, with pure solid Co_3O_4, by the reaction:

$$2\ Co_3O_4 + 6\ Na_2SO_4 = 6\ CoSO_4 + 6\ Na_2O + O_2 \qquad (15)$$

At 1200°K, for a Co_3O_4 saturated solution ($a_{Co_3O_4} = 1$).

$$K_{15} = 1.7992 \times 10^{-90} = \frac{(a_{CoSO_4})^6 (a_{Na_2O})^6\ P_{O_2}}{(a_{Na_2SO_4})^6} \qquad (16)$$

At p_{O_2} of one atmosphere, and assuming a regular solution model for the solution of $CoSO_4$ in Na_2SO_4, Eq. (16) can be written as

$$\log K_{15} = 6 \log\left(\frac{x_{CoSO_4}}{x_{Na_2SO_4}}\right) + 6 \log a_{Na_2O} + 6\frac{\omega_L}{RT}(1-x^{(1)}_{CoSO_4})^2 - 6\frac{\omega_L}{RT}(1-x^{(1)}_{Na_2SO_4})^2 \quad (17)$$

Substituting the value of ω_L calculated from the phase diagram in Eq. (17), a_{Na_2O} is calculated for different points on the solubility curve, and a comparison is made between the calculated and experimental Na_2O activities, which is shown in Table III.

There is close agreement between the thermodynamic properties derived from the phase diagram, and those obtained from the solubility measurements of Gupta and Rapp (7): the small difference between the calculated and experimental values is within the limit of experimental uncertainties.

3.2. P_{SO_3} necessary for liquid formation

CoO and Co_3O_4 are the two oxides that can be formed on oxidizing cobalt. The sulphation reactions for CoO and Co_3O_4 are, respectively:

$$CoO + SO_3 = CoSO_4 \quad (18)$$

$$K_{18} = \frac{a_{CoSO_4}}{p_{SO_3}} \tag{19}$$

$$CoO + SO_2 + \frac{1}{2} O_2 = CoSO_4 \tag{20}$$

$$K_{20} = \frac{a_{CoSO_4}}{p_{SO_2} (p_{O_2})^{1/2}} \tag{21}$$

$$Co_3O_4 + 3SO_3 = 3CoSO_4 + \frac{1}{2} O_2 \tag{22}$$

$$K_{22} = \frac{(a_{CoSO_4})^{1/2} \quad (p_{O_2})^{1/2}}{(p_{SO_3})^3} \tag{23}$$

$$Co_3O_4 + 3SO_2 + O_2 = 3CoSO_4 \tag{24}$$

$$K_{24} = \frac{(a_{CoSO_4})^3}{(p_{SO_2})^3 (p_{O_2})} \tag{25}$$

The activity coefficient of $CoSO_4$ in the liquid can be estimated from Eq. (6), and the p_{SO_2} levels necessary for liquid formation from Na_2SO_4-CoO and Na_2SO_4-Co_3O_4 mixtures can be calculated from Eqs. (18)-(25). (Wherever oxygen is involved in the reaction a p_{O_2} of 0.21 is assumed.)

Figures 3 and 4 show the p_{SO_3} required for liquid formation at different temperatures, from mixtures of Na_2SO_4 -

CoO and Na_2SO_4 - Co_3O_4, respectively. Equilibrium in the O_2-SO_2-SO_3 gaseous mixture has been assumed. The p_{SO_2} and total gaseous sulfur contents coresponding to the p_{SO_3} shown in Figs. 3 and 4 (and subsequent figures) are calculated in the appendix. The minimum p_{SO_3} required for liquid formation goes through a maximum at 850°C. Extremely low p_{SO_3} in the atmosphere is sufficient for the formation of a liquid melt (at 1000°K, for example, the p_{SO_3} required for liquid formation in Na_2SO_4 - CoO, and Na_2SO_4 - Co_3O_4 mixtures are 19 ppm and 60 ppm, respectively), which is consistent with the hot corrosion observed in burner rig tests with low SO_2/SO_3 levels.

Jones (2) has reported experimental determinations of the minimum p_{SO_2} required for Na_2SO_4 - $CoSO_4$ liquid formation at 1000°K in Na_2SO_4 - Co_3O_4 mixture, and their measured p_{SO_2}(≃ 200 ppm) is higher than the values calculated here, p_{SO_2}(≃ 80 ppm) minimum. However, there is no real contradiction between the two values, since Jones may well have formed the liquid with a higher $CoSO_4$ concentration than the minimum required for liquid formation.

4. <u>Na_2SO_4 - $NiSO_4$ System</u>

The Na_2SO_4 - $NiSO_4$ phase diagram (6) is shown in Fig. 5 and all the calculations are made for the Na_2SO_4-rich portion of the phase diagram. Assuming an ideal solid solution behavior, the ω_L values in the salt melt has been estimated at

various temperatures from Eq. (7) (assuming $\omega_S = 0$), and are shown in Table IV.

From Table IV an average value of -6.5 ± 1 Kcal/mole can be estimated for ω_L in the temperature range 700-800°C. In a manner analogous to that of the Na_2SO_4 - $CoSO_4$ system, the liquidus composition can be calculated from Eq. (14), taking the estimated ω_L value (-6.5 ± 1 Kcal/mole). A comparison between the calculated liquidus composition and that obtained from the phase diagram is shown in Table V.

There is close agreement between the two different sets of values at all the temperatures. At 850°C, the ω_L value estimated from the phase diagram is more negative than the average ω_L, but as can be seen from Table V, the estimated average ω_L (-6.5 ± 1 Kcal/mole) does not introduce any significant difference between the calculated liquidus composition and that obtained from the phase diagram. In the dilute solution region the ω_L value is highly sensitive to the composition of the solute, and any small error in the phase diagram determination might have led to a large negative value for ω_L at 850°C.

Gupta and Rapp (7) have also measured the solubility of NiO in molten Na_2SO_4 at 1200°C, at different a_{Na_2O} (Fig. 6), and in the acidic regime NiO can dissolve as $NiSO_4$, which is formed by the reaction

$$NiO + Na_2SO_4 = NiSO_4 + Na_2O \qquad (26)$$

At 1200°K for a NiO-saturated melt,

$$K_{26} = 5.786 \times 10^{-17} = \frac{a_{NiSO_4} \; a_{Na_2O}}{a_{Na_2SO_4}} \tag{27}$$

Assuming a regular solution model for the salt melt

$$\ln K_{26} = \ln\left(\frac{x_{NiSO_4}(1)}{x_{Na_2SO_4}(1)}\right) + \ln a_{Na_2O} + \frac{\omega_L}{RT}\,(1-x_{NiSO_4}(1))^2 - \frac{\omega_L}{RT}\,(1-x_{Na_2SO_4}(1))^2 \tag{28}$$

Taking ω_L the same as that calculated from the phase diagram (-6.5 Kcal/mole), Na_2O is calculated at different data points on the solubility curve, and the calculated values are in close agreement with those of Gupta and Rapp. This is shown in Table VI.

The sulfation reaction for NiO can be written as

$$NiO + SO_3 = NiSO_4 \tag{29}$$

$$K_{29} = \frac{a_{NiSO_4}}{p_{SO_3}} \quad , \tag{30}$$

for a NiO saturated melt. Assuming the regular solution model for the salt melt, a_{NiSO_4} at the liquidus composition can be calculated and the p_{SO_3} required for liquid formation can be estimated from Eq. (30). Figure 7 shows the p_{SO_3} necessary for liquid formation in the $NaSO_4$ - $NiSO_4$ system. (Equivalent p_{SO_2} and total sulfur are again calculated in the Appendix.) The p_{SO_3} level necessary for liquid formation from a Na_2SO_4-NiO mixture is higher than that required for Na_2SO_4-$CoSO_4$ liquid formation, which is primarily responsible for the greater corrosion resistance of Ni-based alloys in comparison to cobalt-based alloys in the temperature range 700-750°C, as has been observed (8).

5. Na_2SO_4 - $Fe_2(SO_4)_3$ System

Figure 8 shows the Na_2SO_4 - $Fe_2(SO_4)_3$ phase diagram (6). For the Na_2SO_4-rich portion of the phase diagram, assuming an ideal solid solution behavior, estimates of ω_L can be obtained, and are shown in Table VII.

The large negative value of ω_L obtained for all the cases is indicative of strong complex formation in the salt melt. Recently, Hendry and Lees (9), in their experiments on corrosion of steels in molten Na_2SO_4 - K_2SO_4 melts, have estimated an activity coefficient of the order of 1.5×10^{-12} for $Fe_2(SO_4)_3$ in the melt, which is also indicative of a strong attractive interaction between $Fe_2(SO_4)_3$ and melt components, possibly leading to complex formation in the melt.

Some information about the nature of the complex species involved in Na_2SO_4 - $Fe_2(SO_4)_3$ melts can be obtained by comparing the activities of $Fe_2(SO_4)_3$ obtained from the phase diagram with that derived using Eq. (12), assuming different complex species in the melt. In the dilute solid solution region, e.g., in the 850-750°C temperature range, the activities obtained from the phase diagram data are in good agreement with those estimated by assuming $Na_3Fe(SO_4)_3$ or ($3Na_2SO_4$ - $Fe_2(SO_4)_3$) as the complex species in the melt, formed by the reaction,

$$3\ Na_2SO_4 + Fe_2(SO_4)_3 = 2\ Na_3Fe(SO_4)_3 \tag{31}$$

At equilibrium the mole fraction of the components in the melt are

$$x'_{Na_2SO_4} = \frac{x_{Na_2SO_4} - 3n_2}{1 - 2n_2} = a_{Na_2SO_4}(1) \tag{32}$$

$$x'_{Fe_2(SO_4)_3} = \frac{x_{Fe_2(SO_4)_3} - n_2}{1 - 2n_2} \tag{33}$$

$$x'_{Na_3Fe(SO_4)_3} = \frac{2n_2}{1 - 2n_2} \tag{34}$$

where n_2 = the number of moles of $Fe_2(SO_4)_3$ consumed by reaction (31). The apparent equilibrium constant for the reaction (31) can be expressed as

$$K_{(31)} = \frac{4n_2^2(1 - 2n_2)^2}{(x_{Na_2SO_4} - 3n_2)^3(x_{Fe_2(SO_4)_3} - n_2)} \qquad (35)$$

The K_{31} estimated for reaction (31) at different temperatures is shown in Table VIII.

The plot of ln K_{31} vs 1/T in the temperature range 850–775°C yields a straight line, which is shown in Fig. 9. Depending on concentration and temperature, several other complex species with different $Fe_2(SO_4)_3$ - Na_2SO_4 coordination can be formed along with $Na_3Fe(SO_4)_3$, and the species with lower Na_2SO_4 - $Fe_2(SO_4)_3$ ratio will be favored at higher $Fe_2(SO_4)_3$ concentrations in the melt, e.g., $NaFe(SO_4)_2$ and so on.

The sulfation reaction of Fe_2O_3 can be described by the reaction

$$Fe_2O_3 + 3\ SO_3 = Fe_2(SO_4)_3 \qquad (36)$$

$$K_{(36)} = \frac{a_{Fe_2(SO_4)_3}}{(p_{SO_3})^3} = \frac{x_{Fe_2(SO_4)_3}\ \gamma_{Fe_2(SO_4)_3}}{(p_{SO_3})^3}$$

The activity of $Fe_2(SO_4)_3$ in the melt can be estimated from Eq. 36, if all the complex forming species at each temperature and

concentration are known. However, in the absence of such information, the regular solution approximation can be made to estimate $\gamma_{Fe_2(So_4)_3}$ in the melt. From Table VII it can be seen that the interaction energy parameter increases with decrease in temperature. For these calculations, an average value of the interaction energy parameter is used, and this is estimated to be -35.383 Kcal/mole. In a manner similar to that of Na_2SO_4 and Na_2SO_4 - $CoSO_4$ systems, the liquidus composition based on the average value of the interaction energy parameter and an ideal solid solution assumption, is calculated and compared with the phase diagram data, which are shown in Table IX.

There seems to be close agreement between the calculated liquidus composition and that obtained directly from the phase diagram, in the temperature range 850-750°C. A change in the value of the interaction energy parameter by ±5 Kcal/mole seems to have no significant effect on the liquidus composition in the temperature range 850-750°C, and thus adopting the average value of the interaction energy parameter for activity calculations is justified.

From Eq. (37), p_{SO_3} required for liquid formation can be calculated, and is shown in Fig. 10. In the temperature range of 650-700°C, p_{SO_3} of the order of 10^{-4} atm is sufficient for Na_2SO_4 - $Fe_2(SO_4)_3$ liquid formation, which could still be in the gas turbine operation range. However, above 700°C liquid formation is not possible under normal gas turbine operating conditions. Burner rig tests (8) have also shown hot corrosion

attack for Fe-based alloys, which could be due to a liquid formation at low temperatures.

6. $Na_2SO_4 - Al_2(SO_4)_3$ System

Figure 11 shows the phase diagram for the Na_2SO_4 - $Al_2(SO_4)_3$ system (6). In the Na_2SO_4-rich terminal solid solution region, the solid solubility of $Al_2(SO_4)_3$ in Na_2SO_4 is extremely small. (At the eutectic temperature, only 2 mole percent of $Al_2(SO_4)_3$ can be dissolved in the solid solution.) Thus, it would seem appropriate to assume an ideal solid solution behavior. Estimates of the interaction energy parameter in the salt melt, assuming an ideal solid solution behavior, is shown in Table X.

The large negative value of the interaction energy parameter again indicates a strong tendency for complex formation in the Na_2SO_4 - $Al_2(SO_4)_3$ melt. There is a wide variation in the values of the interaction energy parameter estimated from the phase diagram, at different temperatures, and ω_L becomes less negative with decrease of temperature. Stroud and Rapp (10) have measured the solubility of Al_2O_3 in Na_2SO_4 melts at 1200°K, and from their solubility data in the acidic regime, where Al_2O_3 dissolves as $Al_2(SO_4)_3$, an estimate of the activity coefficient of $Al_2(SO_4)_3$ in the melt, and the interaction energy parameter can be obtained which is shown in Table XI.

The interaction energy parameter appears to have a strong concentration dependence, and the ω_L value becomes less negative with increase in concentration of $Al_2(SO_4)_3$ in the melt. This can be explained on the basis of the complex formation model, e.g., at low concentration of $Al_2(SO_4)_3$ in the melt, the complex species of higher Na_2SO_4:$Al_2(SO_4)_3$ ratio will be favored, and the ratio of Na_2SO_4 to $Al_2(SO_4)_3$ in the complex will decrease with increase in $Al_2(SO_4)_3$ concentration. Thus, from Eq. (12) a decrease in the activity coefficient of $Al_2(SO_4)_3$ in the melt would be expected as the concentration of $Al_2(SO_4)_3$ increases. The wide variation in the calculated interaction energy parameter can also be explained on the basis of a strong concentration dependence of ω_L. With decrease in temperature, the concentration of $Al_2(SO_4)_3$ as the liquidus composition increases and, based on a complex formation model, the activity coefficient of $Al_2(SO_4)_3$ would be expected to decrease, thus resulting in a less negative value for the interaction energy parameter.

The activity of $Al_2(SO_4)_3$ in the melt, derived from the phase diagram at 850°C and 800°C, agrees well with the activity calculated on the basis of complex formation model (Eq. (12)), assuming $Na_3Al(SO_4)_3$ or 3 Na_2SO_4 - $Al_2(SO_4)_3$ as the complex species formed by the reaction:

$$3\ Na_2SO_4 + Al_2(SO_4)_3 = 2\ Na_3Al(SO_4)_3 \qquad (38)$$

If it is assumed that all the $Al_2(SO_4)_3$ in the melt is consumed to form the complex, then at equilibrium:

$$a_{Na_2SO_4} = \frac{x_{Na_2SO_4}}{x_{Na_2SO_4} - x_{Al_2(SO_4)_3}} \tag{39}$$

where $x_{Na_2SO_4}$ and $x_{Al_2(SO_4)_3}$ are the initial mole fractions of Na_2SO_4 and $Al_2(SO_4)_3$ in the melt, respectively. Table XII shows the comparison between the activities derived from the complex formation model and that obtained from the phase diagram at 850°C and 800°C.

Since a series of different complexes can be formed in the melt for which no information exists, the $a_{Al_2(SO_4)_3}$ in the melt cannot be calculated on the basis of the complex formation model. For the present purpose of calculating the p_{SO_3} required for liquid formation in the Na_2SO_4 - $Al_2(SO_4)_3$ system, an average value of the interaction energy parameter will be estimated. Since the temperature range of 700-800°C is the prime concern in the low-temperature hot-corrosion process, the value of the interaction energy parameter at 750°C will be taken as the average value, e.g., -52.5 Kcal/mole. In a manner analogous to that of the Na_2SO_4 - $CoSO_4$ and Na_2SO_4 - $NiSO_4$ systems, the liquidus composition at each temperature can be calculated, based on the average value of ω_L, which is shown in Table XIII.

There is close agreement between the two sets of values of the liquidus composition, and so the average value of ω_L of -55.2 Kcal/mole will be used to calculate the p_{SO_3} required for liquid formation at all the temperatures in the range 650-850°C.

The sulfation reaction for Al_2O_3 can be written as

$$Al_2O_3(s) + 3\ SO_3(g) = Al_2(SO_4)_3(l) \qquad (40)$$

For the melt saturated with Al_2O_3,

$$K_{40} = \frac{a_{Al_2(SO_4)_3}}{(p_{SO_3})^3} \qquad (41)$$

The p_{SO_3} required for liquid formation at different temperatures is shown in Fig. 12. At temperatures in the range of 700-750°C, p_{SO_3} levels of the order of 10^{-4} atm is sufficient for liquid formation from a mixture of Na_2SO_4 - Al_2O_3, and this level of p_{SO_3} can be attained in the normal range of gas turbine operation.

7. $\underline{Na_2SO_4 - Cr_2(SO_4)_3\ System}$

At present, the phase diagram for Na_2SO_4 - $Cr(SO_4)_3$ is not available. Also, phase diagrams do not exist for other alkali sulfate $Cr_2(SO_4)_3$ systems. However, because of the

importance of Cr as a major alloying element for hot corrosion resistance, an attempt will be made to obtain an approximate estimate of the p_{SO_3} required for $Na_2SO_4 - Cr_2(SO_4)_3$ liquid formation.

The sulfation reaction for Cr_2O_3 can be written as

$$Cr_2O_3(s) + 3\ SO_3(s) = Cr_2(SO_4)_3(l) \tag{42}$$

Assuming a regular solution model, the p_{SO_3} required for liquid formation can be expressed as

$$\ln p_{SO_3} = \frac{1}{3}[\ln x_{Cr_2(SO)_3}^{(l)} + \frac{\omega_L}{RT}(1-x_{Cr_2(SO_4)_3}^{(l)})^2 - \ln K_{42}] \tag{43}$$

Stroud and Rapp (10) and Liang and Elliott (11) have experimentally determined the solubility of Cr_2O_3 in molten Na_2SO_4 at 1200°K, and from their solubility data an average value of -14.31 Kcal/mole for the interaction energy parameter for $Na_2SO_4 - Cr_2(SO_4)_3$ melt can be estimated and can be substituted in Eq. (43) to calculate the p_{SO_3}. In the absence of any other information, reasonable approximation of the liquidus composition at different temperatures can be made by assuming a similar pattern for $Na_2SO_4 - Cr_2(SO_4)_3$ and other $Na_2SO_4 - M_2(SO_4)_3$ (M = Fe or Al) phase diagrams. In the present study, the liquidus composition is approximated to be the

same as that of Na_2SO_4 - $Fe(SO_4)_3$ and Na_2SO_4 - $Al_2(SO_4)_3$ system, and the p_{SO_3} required for liquid formation for each case is calculated separately. These are shown in Fig. 13. For both cases, at temperatures of the order of 750°C, the p_{SO_3} required for liquid formation is about 0.01 atm, which is normally not attained in gas turbine operation. Thus, it would be expected that alloys containing high Cr will have significant resistance to hot-corrosion attack.

8. Interaction of Na_2SO_4 - MSO_4 (M = Co, Ni) Melts with the Protective Oxides Al_2O_3 and Cr_2O_3

The oxidation behavior of resistant alloys, which at high temperatures normally rely for their protection on the formation of a continuous layer of Al_2O_3 or Cr_2O_3, in this lower temperature range of 650-800°C has not been well-characterized. However, it is anticipated that formation of a continuous layer of the protective oxide will be difficult at least in the early stages of oxidation; thus formation of the base metal oxides NiO or CoO will continue for some appreciable time. As a consequence, the early stages of the low-temperature hot-corrosion process is considered to be the formation of Na_2SO_4 - MSO_4 (M = Co, Ni) melts, while the subsequent propagation process depends on the interaction of this melt with the protective oxides Al_2O_3 and Cr_2O_3 themselves.

The possible reactions betwen the mixed sulfate melt and Cr_2O_3 or Al_2O_3 can be expressed as:

(M - Co or Ni)

$$MSO_4 + Al_2O_3 = MAl_2O_4 + SO_3 \tag{44}$$

$$K_{44} = \frac{p_{SO_3}}{a_{MSO_4}} \quad , \tag{45}$$

for melts saturated with MAl_2O_4 and Al_2O_3.

$$MSO_4 + Cr_2O_3 = MCr_2O_4 + SO_3 \tag{46}$$

$$K_{46} = \frac{p_{SO_3}}{a_{MSO_4}} \quad , \tag{47}$$

for melts saturated with MCr_2O_4 and Cr_2O_3.

$$3\ MSO_4 + 4\ Al_2O_3 = Al_2(SO_4)_3 + 3\ MAl_2O_4 \tag{48}$$

$$K_{48} = \frac{a_{Al_2(SO_4)_3}}{(a_{MSO_4})^3} \tag{49}$$

for melts saturated with Al_2O_3 and MAl_2O_4

$$3\ MSO_4 + 4\ Cr_2O_3 = Cr_2(SO_4)_3 + 3\ MCr_2O_4 \tag{50}$$

$$K_{50} = \frac{a_{Cr_2(SO_4)_3}}{(a_{MSO_4})^3} \quad , \tag{51}$$

for melts saturated with Cr_2O_3 and MCr_2O_4.

$$Na_2SO_4 + Al_2O_3 = 2\ NaAlO_2 + SO_3 \tag{52}$$

$$K_{52} = \frac{p_{SO_3}}{a_{Na_2SO_4}} \quad , \tag{53}$$

for melts saturated with Al_2O_3 and $NaAlO_2$.

$$Na_2SO_4 + 1/2\ Cr_2O_3(s) + 3/4\ O_2(g) = Na_2CrO_4 + SO_3(g) \tag{54}$$

$$K_{54} = \frac{p_{SO_3}}{a_{Na_2SO_4}\ (p_{O_2})^{3/4}} \quad , \tag{55}$$

for melts saturated with $Na_2(CrO_4)$.

Reactions (52) and (54) cannot go to the right, under the normal level of SO_3 prevalent in gas turbine operations, and so will not be considered further in the calculations. For reactions (44) and (46), upon fixing the p_{SO_3}, the a_{MSO_4} in the melt saturated with the spinels is automatically fixed from reactions (45) and (47). If instead of a spinel the Al_2O_3 and Cr_2O_3 form their respective sulfates in the melt by reactions (48) and (50), then the activity of MSO_4 in the melt will depend upon the activity of $Al_2(SO_4)_3$ or $Cr_2(SO_4)_3$ in the melt. At a given p_{So_3}, the activity of $Al_2(SO_4)_3$ or $Cr_2(SO_4)_3$ in the melt will be governed respectively by the following equilibria:

$$Al_2O_3 + 3\ SO_3 = Al_2(SO_4)_3 \tag{55}$$

$$K_{55} = \frac{a_{Al_2(SO_4)_3}}{(p_{SO_3})^3} \tag{56}$$

$$Cr_2O_3 + 3\ SO_3 = Cr_2(SO_4)_3 \tag{57}$$

$$K_{57} = \frac{a_{Cr_2(SO_4)_3}}{(p_{SO_3})^3}$$

Thus, the activity of MSO_4 coexisting with $Al_2(SO_4)_3$ or $Cr_2(SO_4)_3$ in the melt can be predicted for different p_{SO_3} levels at each temperature.

Figures 14 and 15 show the equilibrium relationships in the system Na_2SO_4 - $CoSO_4$ - Al_2O_3 - SO_3 and Na_2SO_4 - $CoSO_4$ - Cr_2O_3 - SO_3, respectively. The corresponding equilibrium relations for the Na_2SO_4 - $NiSO_4$ - Al_2O_3 - SO_3 and Na_2SO_4 - $NiSO_4$ - Cr_2O_3 - SO_3 systems are shown in Figs. 16 and 17, respectively. The figures show a plot of log a_{MSO_4} in the melt vs temperature at different p_{SO_3} levels in the atmosphere. Curve (1) shows the equilibrium relationships for reactions (44) and (46), whereas curve (2) shows the equilibrium relationships for reactions (48) and (50). For a particular p_{SO_3}, if the activity of MSO_4 in the Na_2SO_4 - MSO_4 melt lies in the region above the curve (1), the melt will decompose to form MAl_2O_4 and generate SO_3, whereas in the region below curve (1) reactions (44) and (46) will go to the left. Similarly, at a particular p_{SO_3} of the activity of MSO_4 in the Na_2SO_4 - MSO_4 melt lies in the region above curve (2), the MSO_4 component of the melt will react with Al_2O_3 or Cr_2O_3 to form spinels and $Al_2(SO_4)_3$, $Cr_2(SO_4)$, respectively; and in the region below curve (2), Na_2SO_4 - MSO_4 melt can coexist with Al_2O_3 or Cr_2O_3. The chain curve is a plot of log a_{MSO_4} in the melt at the liquidus composition.

Equilibrium considerations for the Na_2SO_4 - $CoSO_4$ - Al_2O_3 - SO_3 system (Fig. 14) show that at a p_{SO_3} range of $2x10^{-4}$ - 10^{-3} atm and temperatures below 725°C, Na_2SO_4 - $CoSO_4$ melt can coexist with either $CoAl_2O_4$ or $CoAl_2O_4$ and $Al_2(SO_4)_3$ in the melt, depending on whether reaction (44) or (48) is the predominant reaction. For example, at 700°C, if the P_{SO_3} is above $8x10^{-4}$ atm, the liquid Na_2SO_4 - $CoSO_4$ can coexist with the spinel and/or $Al_2(SO_4)_3$, whereas if the p_{SO_3} is below $8x10^{-4}$ atm, the a $CoSO_4$ drops below that required for the Na_2SO_4 - $CoSO_4$ liquid to be stable, and thus the liquid will decompose. At temperatures above 725°C, for the Na_2SO_4 - $CoSO_4$ liquid to be stable along with $CoAl_2O_4$ or $CoAl_2O_4$ and $Al_2(SO_4)_3$, more than 10^{-3} atm of p_{SO_3} is necessary, which is not normally attained in gas turbine operation. Although Na_2SO_4 - $CoSO_4$ melt in the presence of Al_2O_3 will decompose above 725°C under normal gas turbine operations, another liquid of Na_2SO_4 - $Al_2(SO_4)_3$ can form if reaction (48) is the predominant reaction. As described earlier in the section on Na_2SO_4 - $Al_2(SO_4)_3$ system, p_{SO_3} in the range of 10^{-3}-10^{-4} atm is sufficient for the formation of a Na_2SO_4 - $Al_2(SO_4)_3$ liquid (Fig. 12). Thus, during the corrosion of cobalt base alloys containing Al, one liquid phase is being replaced by another, as the Na_2SO_4 - $CoSO_4$ melt comes into contact with Al_2O_3, thus making the alloy more vulnerable to hot corrosion attack. At 700°C, the p_{SO_3} level above which Na_2SO_4 -

$CoSO_4$ liquid can coexist with Al_2O_3 and the spinel is of the order of $8x10^{-4}$ atm, which is towards the higher side of the p_{SO_3} level, normally encountered in gas turbine operation, and this is primarily the reason why there are so many conflicting reports concerning the role of aluminum in the overall hot-corrosion process.

The equilibria for the Na_2SO_4 - $CoSO_4$ - Cr_2O_3 - SO_3 system is shown in Fig. 15, and a p_{SO_3} level of the order of 10^{-2} - .1 atm is required for Na_2SO_4 - $CoSO_4$ melt to be stable in contact with Cr_2O_3. Also, a very high level of p_{SO_3} is considered for the Na_2SO_4 - $Cr_2(SO_4)_3$ liquid formation. So under normal gas turbine operating conditions, Na_2SO_4 - $CoSO_4$ melt, upon coming into contact with Cr_2O_3 will decompose to form $CoCr_2O_4$ and generate SO_3 gas by reaction (47).

Figures 16 and 17 show the equilibria for Na_2SO_4 - $NiSO_4$ - Al_2O_3 - $/SO_3$ and Na_2SO_4 - $NiSO_4$ - CR_2O_3 - SO_3, respectively. For both of these systems, the Na_2SO_4 - $NiSO_4$ melt is not stable at all temperatures at a p_{SO_3} level below 10^{-3} atm, but for the melt in contact with Al_2O_3 a Na_2SO_4 - $Al_2(SO_4)_3$ melt can be formed if reaction (48) is the predominant one. However, for the system consisting of Cr_2O_3, formation of Na_2SO_4 - $Cr_2(SO_4)_3$ liquid requires a high p_{SO_3} level (Fig. 13), and $NiCr_2O_4$ will be the only stable phase under normal gas turbine operating conditions.

Summary and Concluding Remarks

The utility of the phase diagrams in predicting the thermodynamic properties of the binary system has been demonstrated for salt melts of importance in the low-temperature hot-corrosion process. The calculated thermodynamic data show satisfactory agreement with most of the available experimental observations. The thermodynamic calculations have also shown that the activity of $Al_2(SO_4)_3$ and $Fe_2(SO_4)_3$ in the melt can be lowered to such an extent that Na_2SO_4 - $Al_2(SO_4)_3$ and Na_2SO_4 - $Fe_2(SO_4)_3$ liquids can be formed at p_{SO_3} levels, that can be attained in the marine gas turbine operations, and this has been explained on the basis of complex formation in the melt. Thermodynamic analysis of the interaction of the Na_2SO_4 - MSO_4 (M = Co or Ni) melt with protective oxides Al_2O_3 and Cr_2O_3, has demonstrated the vulnerability of aluminum-containing alloys to hot-corrosion attack. It appears that the development of a continuous layer of Cr_2O_3 or a $NiCr_2O_4$ spinel layer from the onset of oxidation would improve the hot-corrosion resistance considerably.

Although thermodynamic analysis has shown that Na_2SO_4 - $Al_2(SO_4)_3$ and Na_2SO_4 - $Fe_2(SO_4)_3$ melts can be formed at p_{SO_3} level and temperatures of concern to low-temperature hot-corrosion process, the kinetics of both the formation of mixed sulfates and the reaction of mixed sulfates with the oxides of the alloying elements will eventually be the determining factor in

developing the alloys for improved hot-corrosion resistance. Unfortunately, practically no information currently exists on the kinetics of these important reactions in the hot-corrosion process, and this is an area where further work is required.

ACKNOWLEDGMENTS

This work has been supported by the U.S. Department of Energy, Office of Basic Energy Science, Division of Materials Science, under Contract No. W-7405-Eng-48.

Appendix

SO_2 - O_2 - SO_3 Equilibrium

The equilibria for the SO_2 - O_2 - SO_3 system can be described as

$$SO_2 + \frac{1}{2} O_2 = SO_3 \qquad (A1)$$

$$K_{A1} = \frac{p_{SO_3}}{(p_{SO_2})\,(p_{O_2})^{1/2}}$$

Let $p_{/SO_2^o}$, $p_{O_2^o}$, $p_{N_2^o}$ be the partial pressure of SO_2, O_2, and N_2 respectively in the Air - SO_2 mixture. From the stoichiometry and mass balance consideration for reaction A1, the Equilibrium p_{SO_3} can be obtained by solving the following algebraic equation.

$$\frac{1}{2} p_{SO_3}^3 (K_1^2 - 1) - p_{SO_3}^2 \; (p_{O_2}^o + p_{SO_2}^o)(K_1^2 - 1) - p_{N_2}^o$$

$$+ p_{SO_3} \; \frac{p^2_{SO_2^o}}{2} + 2\, p_{SO_2}^o \cdot p_{O_2}^o$$

$$- K_1^2 \, p_{SO_2}^o \cdot p_{O_2}^o = 0 \,. \qquad (A2)$$

The variation of p_{SO_3} with temperature and initial p_{SO_2} in the Air - SO_2 mixture is shown in Fig. 18.

References

1. J. Balajka and V. Danek, Werk. u. Korrosion 25, 513 (1974).
2. R.L. Jones, A summary and review of NAVSEA-funded low power hot corrosion studies. NRL Memorandum Report 4072, 24 September 1979.
3. D.A. Shores, Annual Report, December 1978, NRL Contract N00173-C-0253, G.E. R and D Laboratory, Schenectady, New York (reference taken from Ref. 2).
4. J. Lumsden, Thermodynamics of molten salt mixtures, Academic Press, London, 1966.
5. I. Prigogine and R. Defay, Chemical thermodynamics, Longmans Green and Co., London, 1954.
6. Phase diagrams for ceramicists. Ed. and Publ. by American Ceramic Society, Inc.
7. D.K. Gupta and R.A. Rapp, This Journal, to be published.
8. A.K. Misra and D.P. Whittle, submitted to Corros. Sci.
9. A. Hendry and D.J. Lees, Corros. Sci. 20, 383 (1980).
10. W.P. Stroud and R.A. Rapp, High temperature metal halide chemistry, Edited by D.L. Hildenbrand, D.D. Cabicciolti, Electrochemical Society, p.547 (1978).
11. W.W. Liang and J.F. Elliott, Properties of high temperature alloys. Edited by Z.A. Fouroulis and F.S. Petit, Electrochemical Society, p. 557 (1976).

TABLE I. Interaction parameters in Na_2SO_4 - $CoSO_4$ liquid solutions.

Temperature °C	W_L, cal/mole
850	-6017
800	-6521
750	-7662
700	-8120
650	-7696
600	-6883

TABLE II. A comparison between calculated liquidus compositions and those obtained from the phase diagram for the Na_2SO_4 - $CoSO_4$ system.

Temperature, °C	$x_{Na_2SO_4}$ (from phase diagram)	$x_{Na_2SO_4}$ (calculated)
850	0.92	0.9218
800	0.83	0.834
750	0.772	0.765
700	0.72	0.709
650	0.664	0.653
600	0.61	0.603

TABLE III. A comparison between calculated and experimental (7) Na_2O activities for Na_2SO_4 - $CoSO_4$ liquid saturated solution.

x_{CoSO_4} (from solubility curve	$x_{Na_2SO_4}$ (from solubility curve)	log a_{Na_2O} (Gupta and Rapp)	Calculated a_{Na_2O} (W_L = -7 Kcal/mole)
0.023	0.977	-12.5	-12.09
0.192	0.808	-13.7	-13.532

TABLE IV. Interaction parameters in Na_2SO_4 - $NiSO_4$ liquid solutions

Temperature, °C	W_L Kcal/mole
850	-16.991
800	-7.876
750	-6.516
700	-5.873

TABLE V. A comparison between calculated liquidus compositions and those obtained from the phase diagram for the Na_2SO_4 - $NiSO_4$ system.

Temperature, °C	$x_{Na_2SO_4}$ (from phase diagram)	$x_{Na_2SO_4}$ (calculated)
850	0.936	0.921
800	0.828	0.821
750	0.75	0.746
700	0.678	0.684

TABLE VI. A comparison between calculated and experimental (7) Na_2O activities for Na_2SO_4 - $NiSO_4$ liquid saturated solutions.

x_{NiSO_4} (from solubility curve)	$x_{Na_2SO_4}$ (from solubility curve)	log a_{Na_2O} (Gupta and Rapp)	Calculated a_{Na_2O} (W_L = -6.5±1 Kcal)
0.023	0.977	-12.5	-12.09
0.192	0.808	-13.7	-13.532

TABLE VII. Interaction parameters in Na_2SO_4 - $Fe_2(SO_4)_3$ liquid solutions.

Temperature, °C	W_L, Kcal/mole
850	-25.422
800	-32.377
750	-36.551
700	-42.798
650	-41.734

TABLE VIII. Apparent equilibrium constant for the reaction $3Na_2SO_4 - Fe_2(SO_4)_3 = 2Na_3Fe(SO_4)_3$.

Temperature, °C	Apparent equilibrium constant
850	0.2043
825	1.395
800	5.338
773	19.894

TABLE IX. A comparison between calculated liquidus compositions and those obtained from the phase diagram for the Na_2SO_4 - $Fe_2(SO_4)_3$ system.

Temperature, °C	$x_{Na_2SO_4}$ (from phase diagram)	$x_{Na_2SO_4}$ (calculated)
850	.94	.946
800	.903	.903
750	.877	.878
700	.862	.853
650	.842	.828

TABLE X. Interaction parameters in the Na_2SO_4 - $Al_2(SO_4)_3$ liquid solutions.

Temperature, °C	W_L, Kcal/mole
850	-89.3
800	-74.506
750	-52.490
700	-38.625
650	-28.762

TABLE XI. Estimates of $\gamma_{Al_2(SO_4)_3}$ and $W_{L_{Na_2SO_4 - Al_2(SO_4)_3}}$ from solubility measurements (11) at 1200°K

$x_{Al_2(SO_4)_3}$ (1)	$\gamma_{Al_2(SO_4)_3}$	W_L
0.0003	9.5×10^{-14}	-71.5
0.003	2.94×10^{-13}	-69.175
0.03	3.383×10^{-12}	-66.52

TABLE XII. A comparison between activities of Na_2SO_4 calculated assuming complex formation, and those from the phase diagram.

Temperature, °C	$a_{Na_2SO_4}$ (l), calculated based on complex formation model	$a_{Na_2SO_4}$ (l), calculated from the phase diagram
850	.927	.921
800	.855	.818

TABLE XIII. Comparison of calculated liquidus compositions with those from the phase diagram for Na_2SO_4 - $Al_2(SO_4)_3$ liquid solutions.

Temperature, °C	$a_{Na_2SO_4}$ (liquidus), calculation	$a_{Na_2SO_4}$ (measured), phase diagram
850	.96	.97
800	.93	.94
750	.91	.91
700	.89	.87
650	.87	.83

Figure Captions

Fig. 1. The Na_2SO_4 - $CoSO_4$ phase diagram (6).

Fig. 2. Solubility of Co_3O_4 in $NaSO_4$ at 1200K after Gupta and Rapp (7).

Fig. 3. Minimum p_{SO_3} required for liquid formation as a function of temperature in the Na_2SO_4 - CoO - SO_3 system.

Fig. 4. Minimum p_{SO_3} required for liquid formation as a function of temperature in the Na_2SO_4 - Co_3O_4 - SO_3 system.

Fig. 5. The Na_2SO_4 - $NiSO_4$ phase diagram (6).

Fig. 6. Solubility of NiO in Na_2SO_4 at 1200K after Gupta and Rapp (7).

Fig. 7. Minimum p_{SO_3} required for liquid formation as a function of temperature in the Na_2SO_4 - NiO - SO_3 system.

Fig. 8. The Na_2SO_4 - $Fe_2(SO_4)_3$ phase diagram (6).

Fig. 9. Equilibrium constant for the reaction 3 Na_2SO_4 + $Fe_2(SO_4)_3$ = 2 $Na_3Fe(SO_4)_3$ as a function of temperature.

Fig. 10. Minimum p_{SO_3} required for liquid formation as a function of temperature in the Na_2SO_4 - $Fe_2(SO_4)_3$ system.

Na_2SO_4–$CoSO_4$

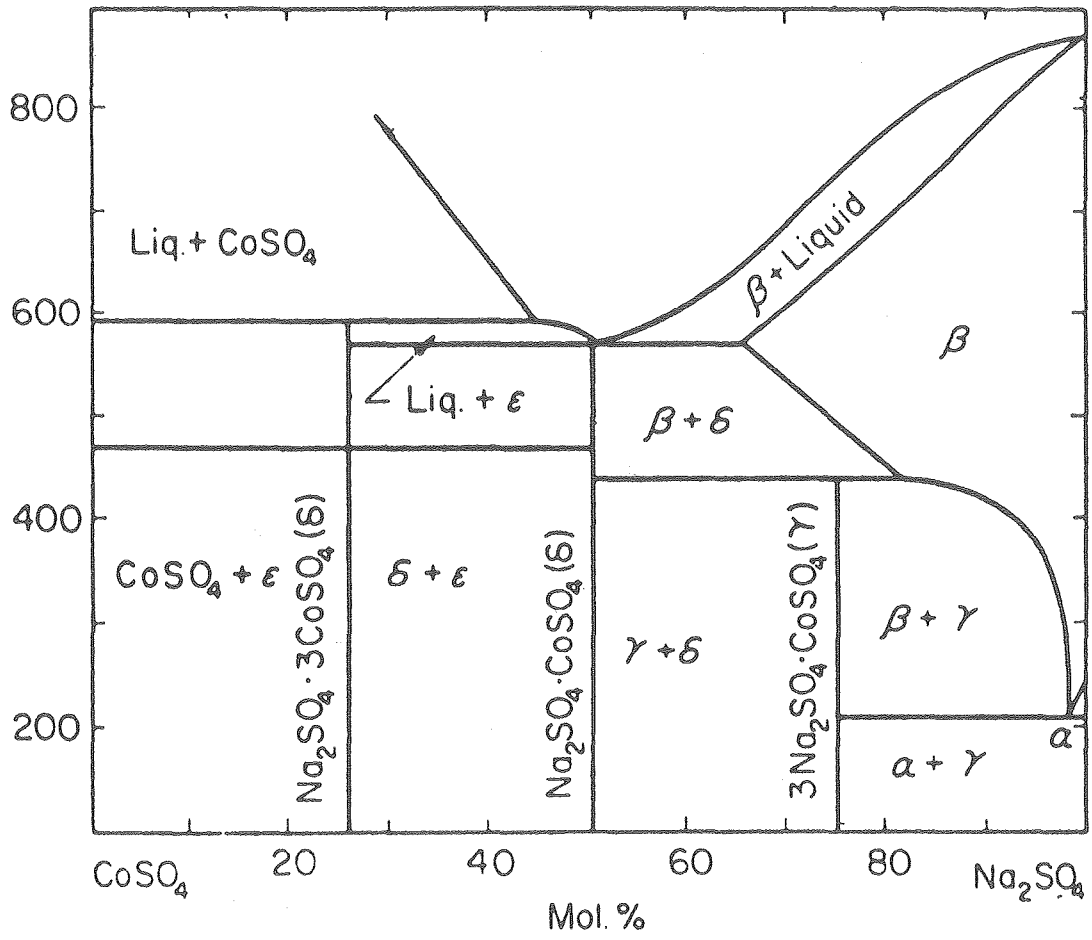

XBL 809-11583

Figure 1

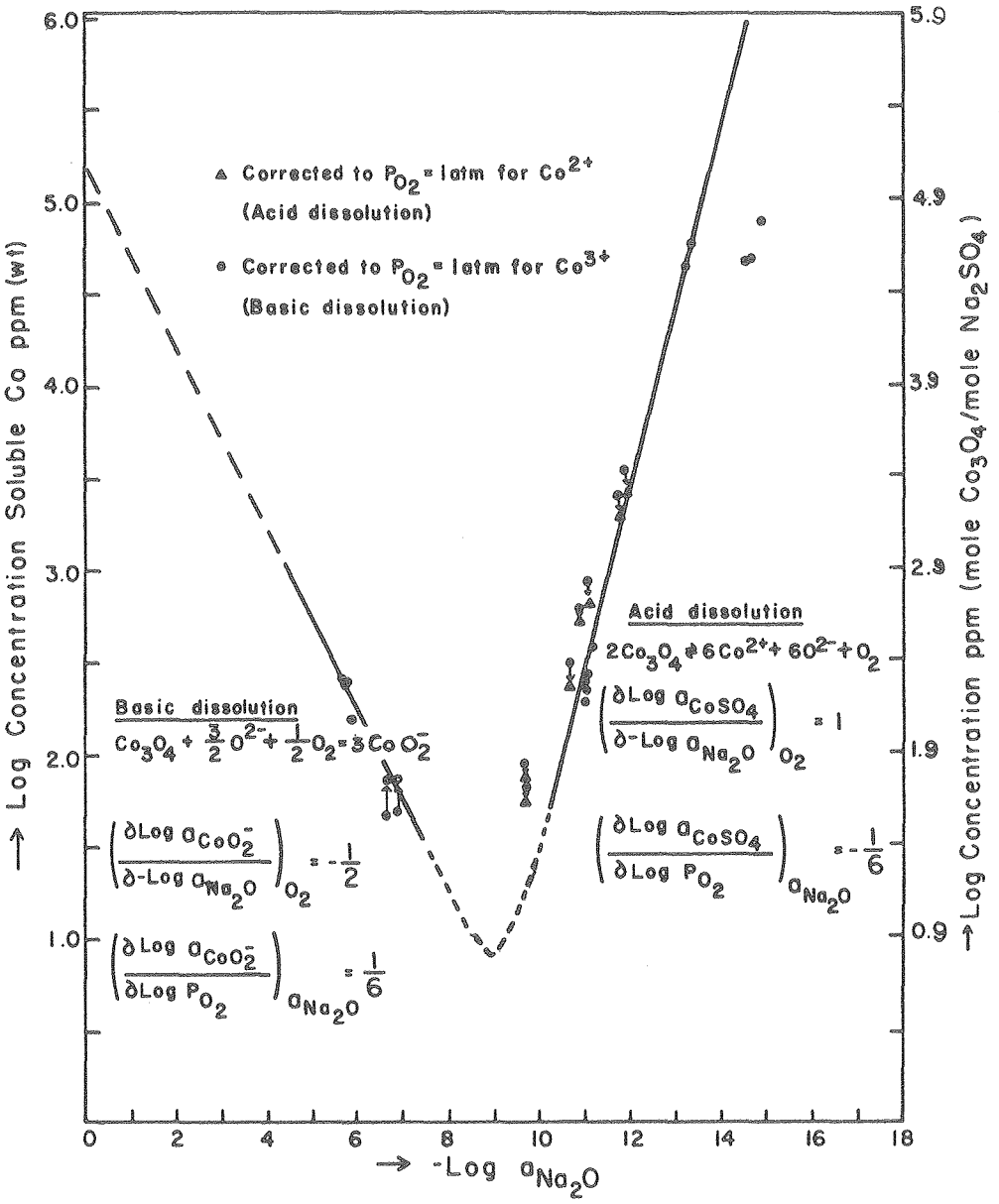

Figure 2

XBL 809-11579

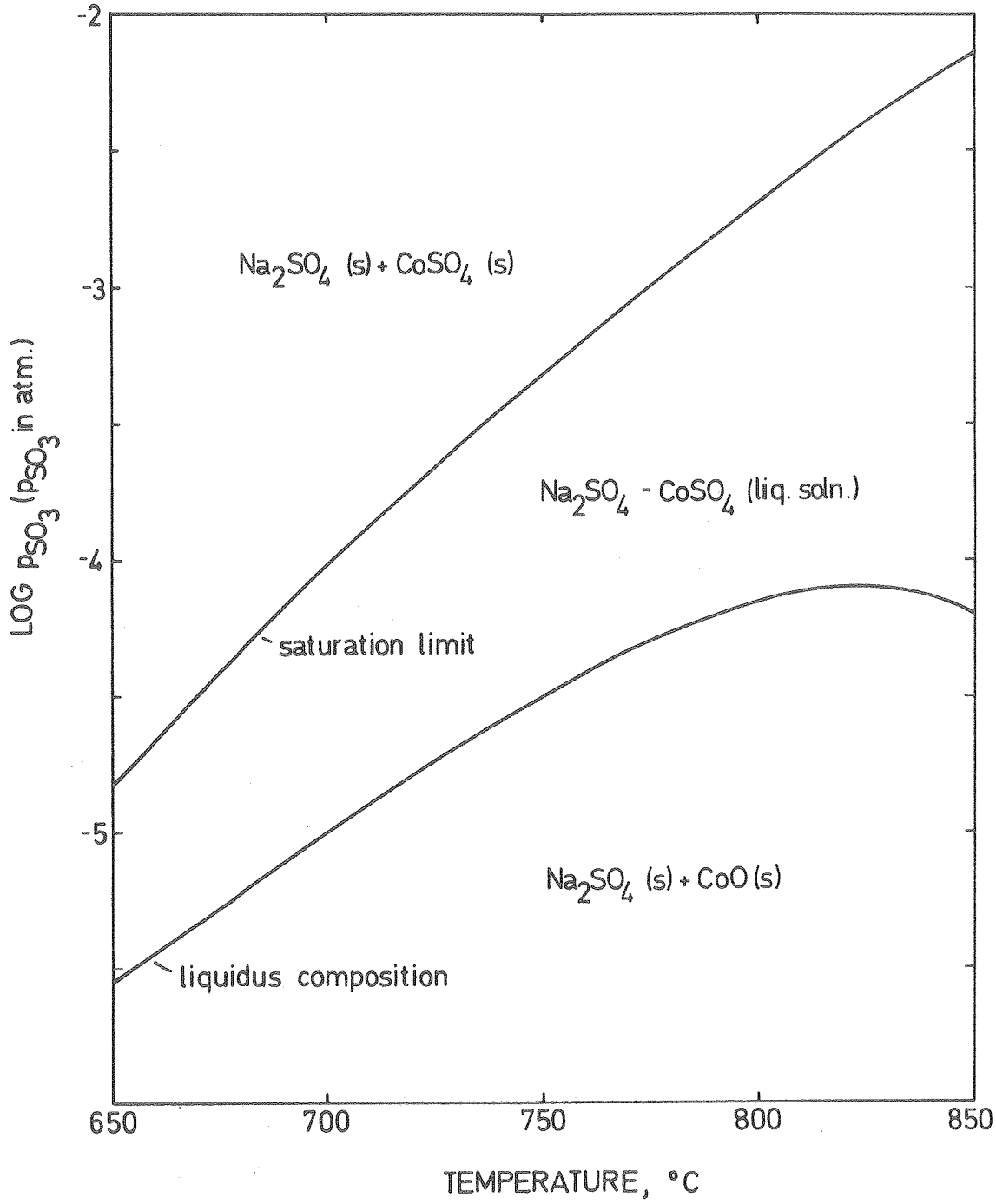

Figure 3

XBL 809-11572

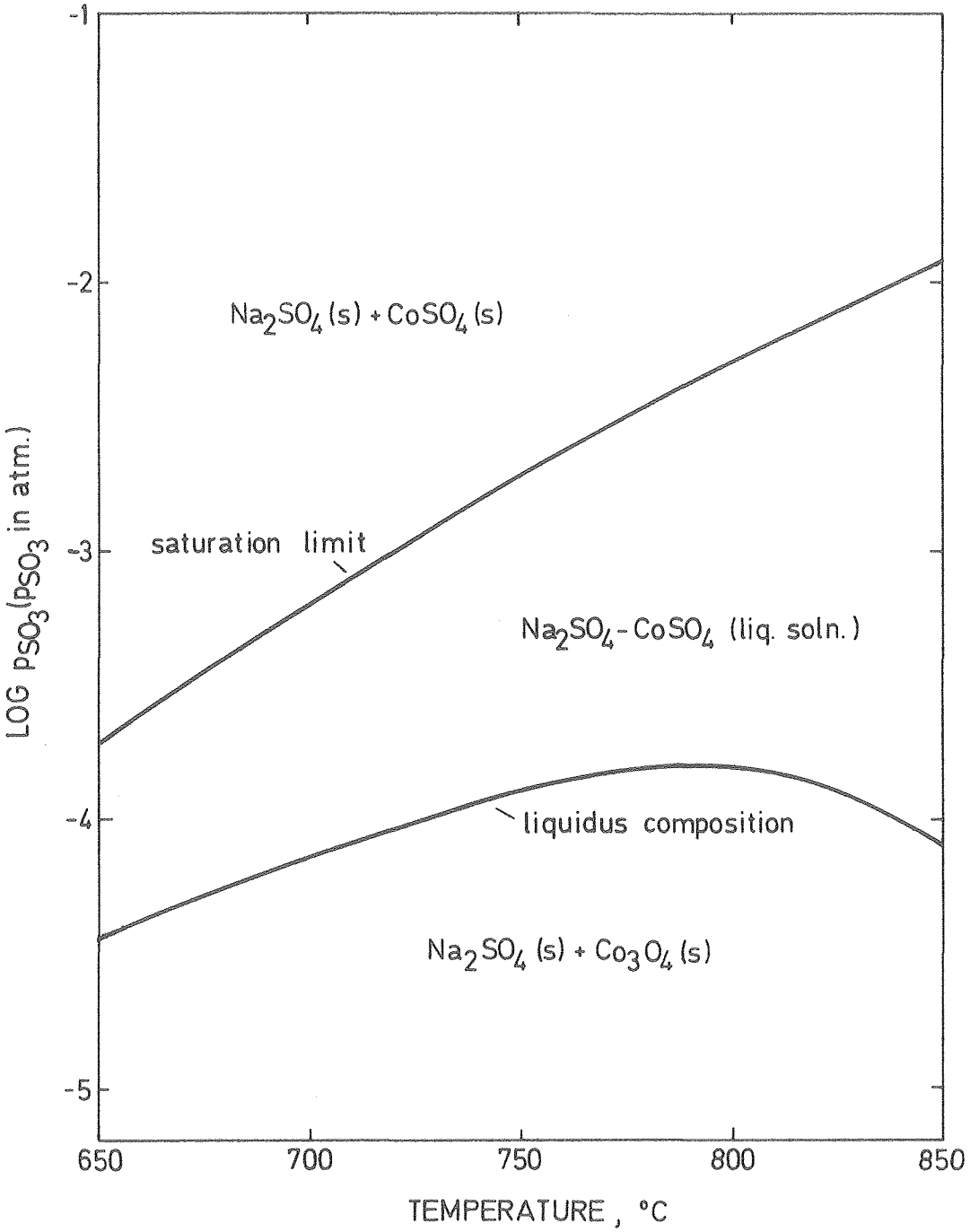

Figure 4

XBL 809-11573

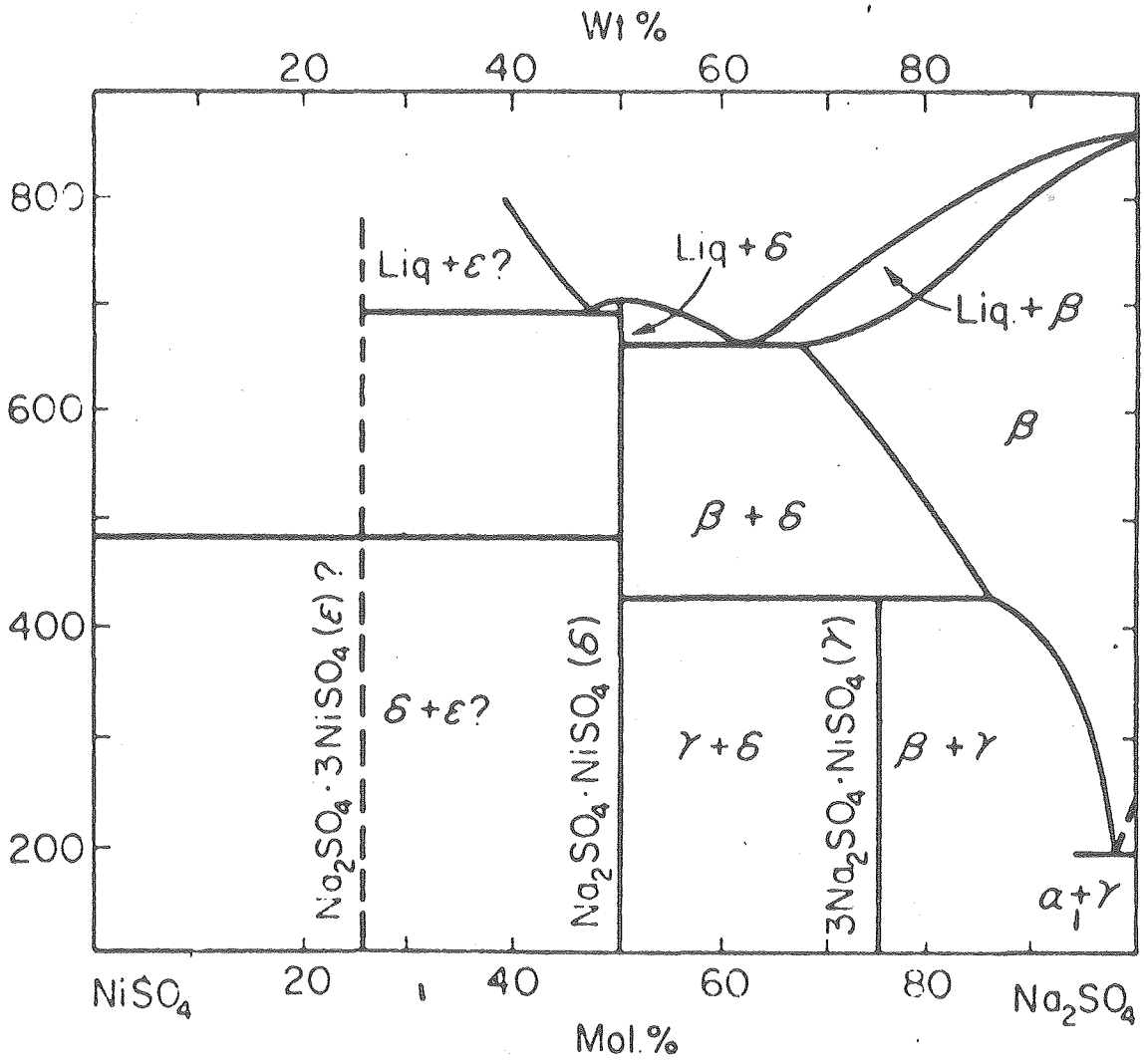

XBL 809-11584

Figure 5

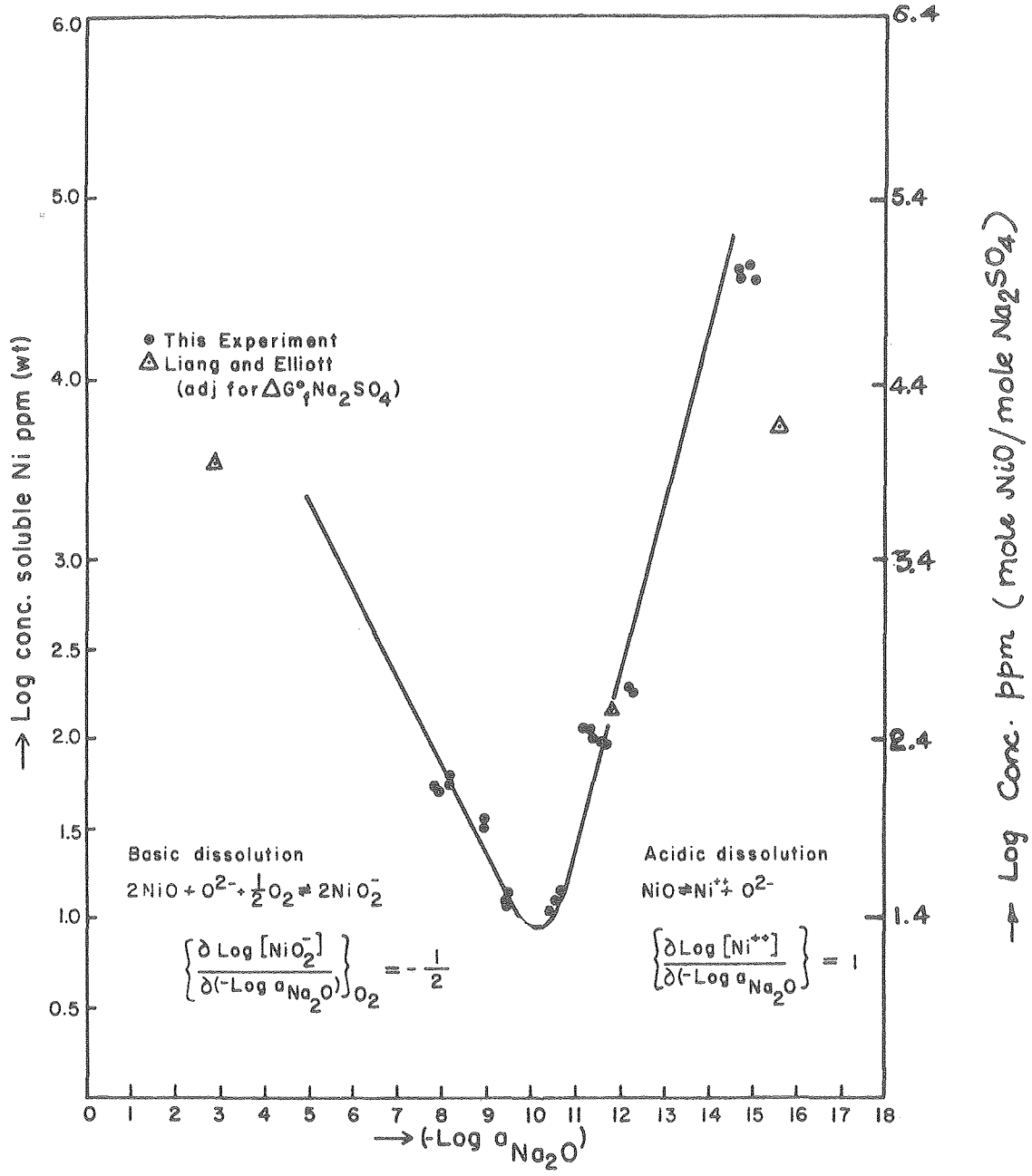

Figure 6

XBL 809-11576

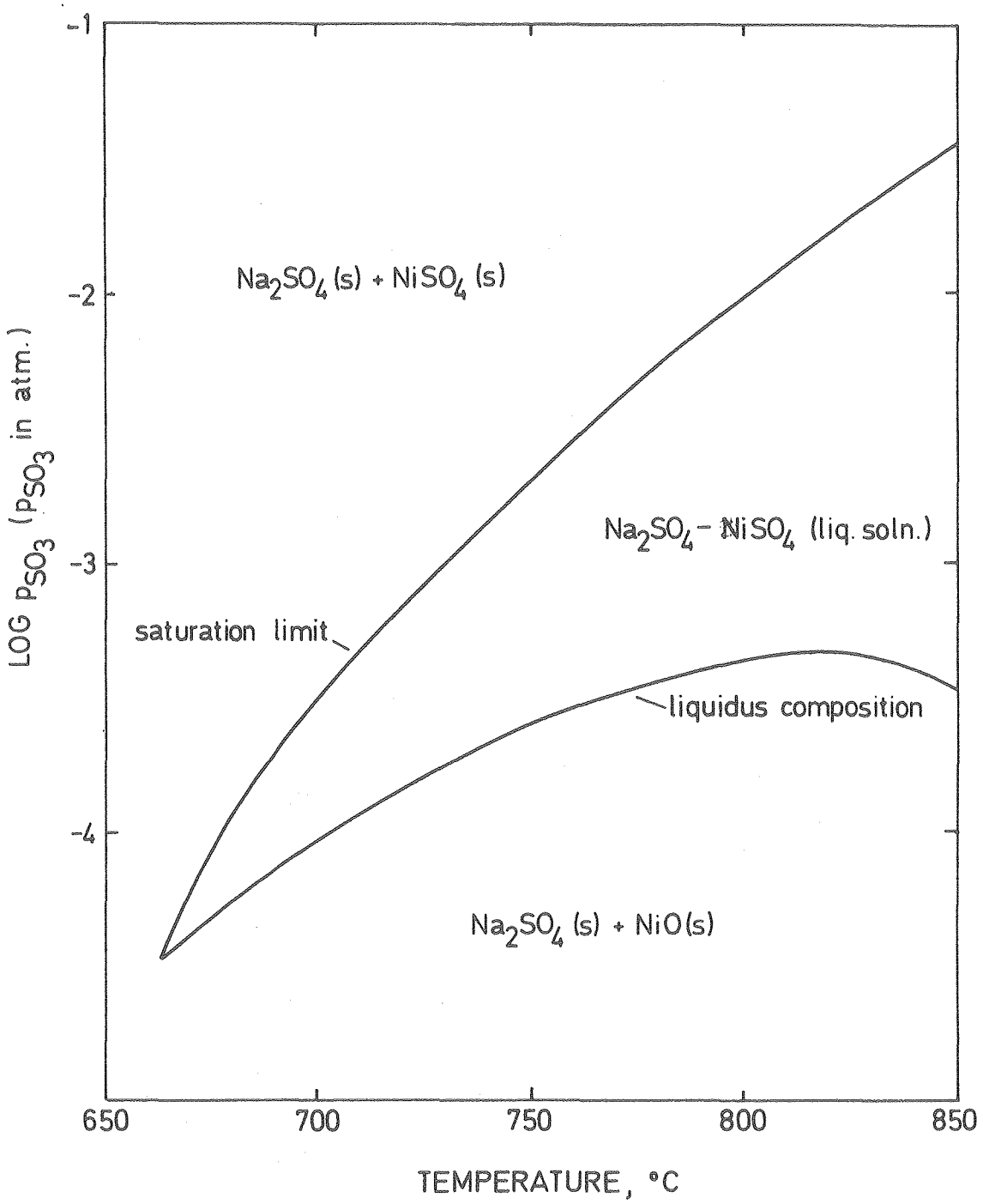

XBL 809-11567

Figure 7

Na_2SO_4–$Fe_2(SO_4)_3$

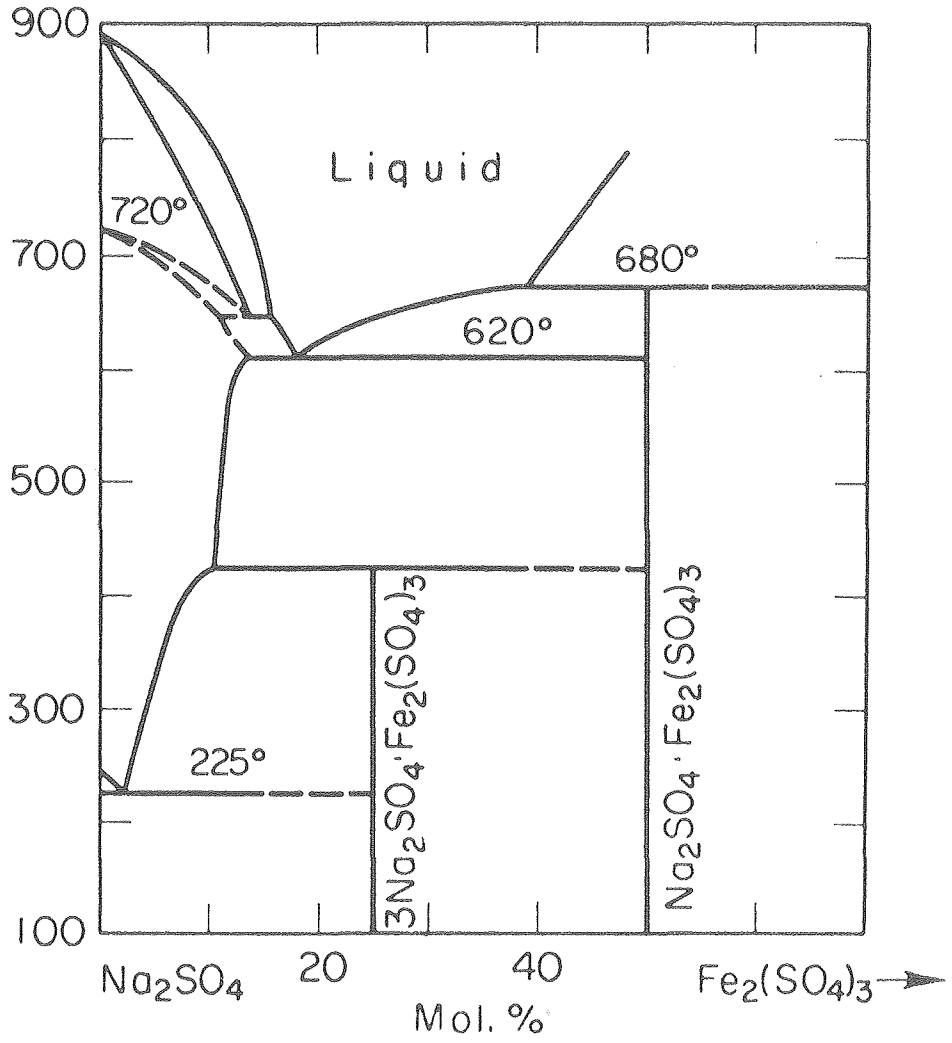

Figure 8

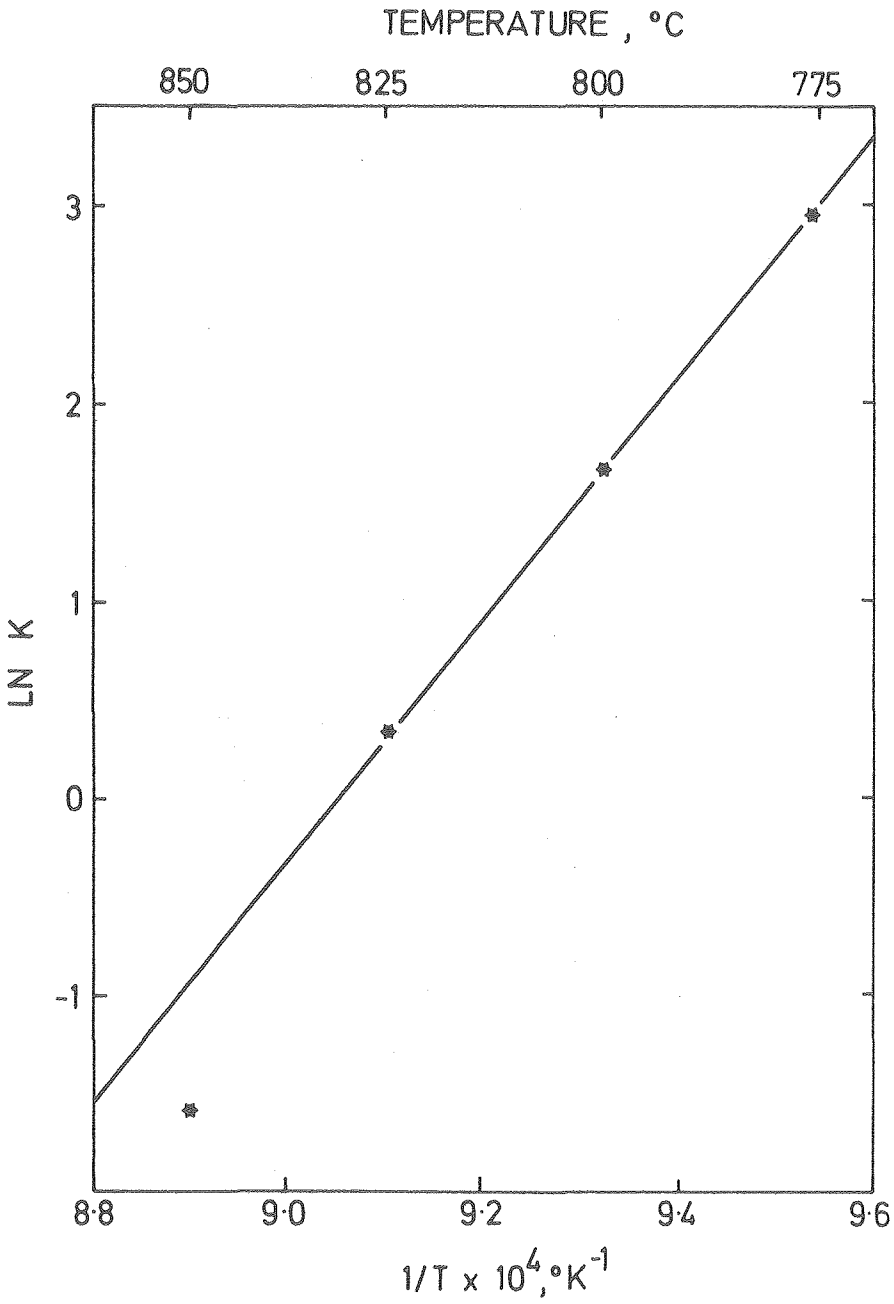

Figure 9

XBL 809-11569

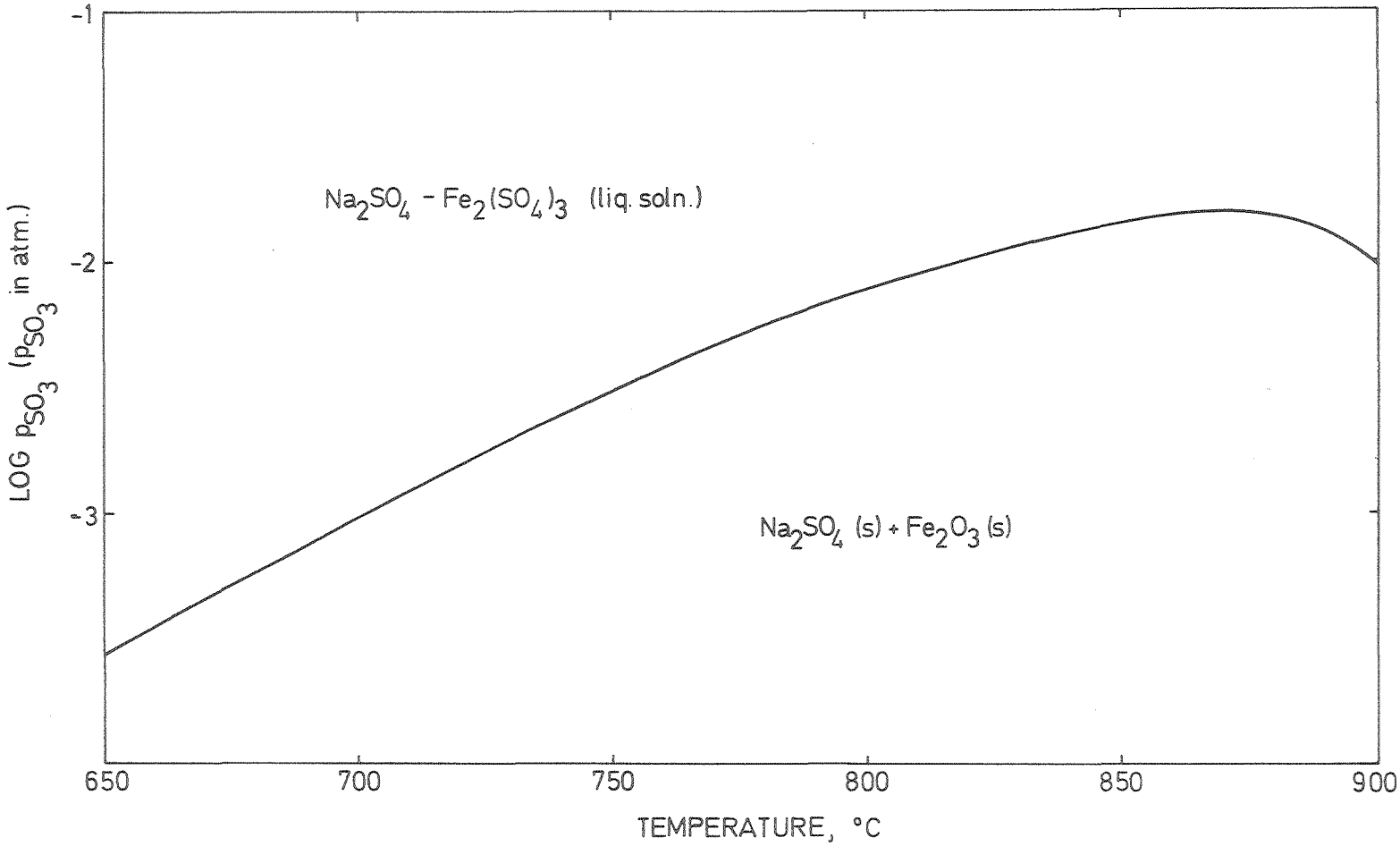

Figure 10

XBL 809-11568

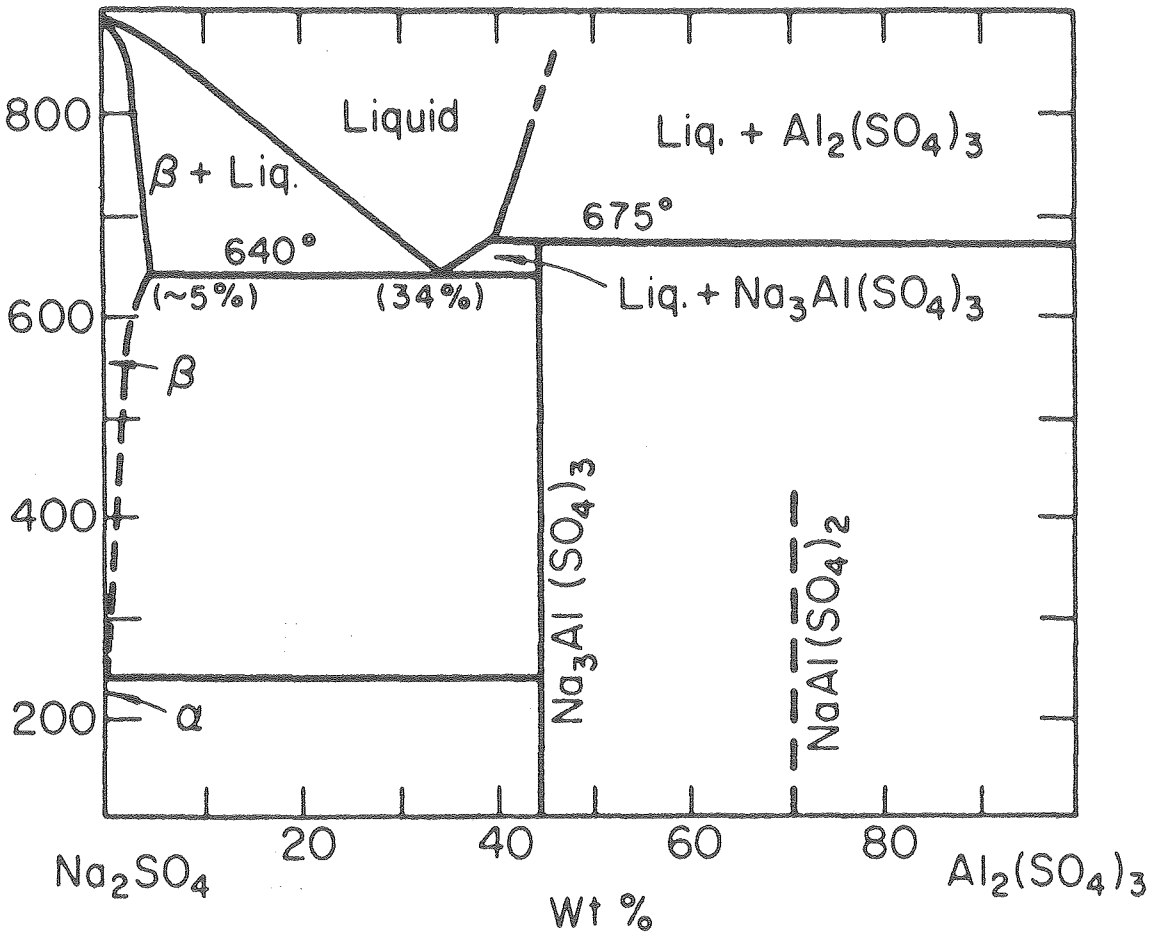

XBL 809-11582

Figure 11

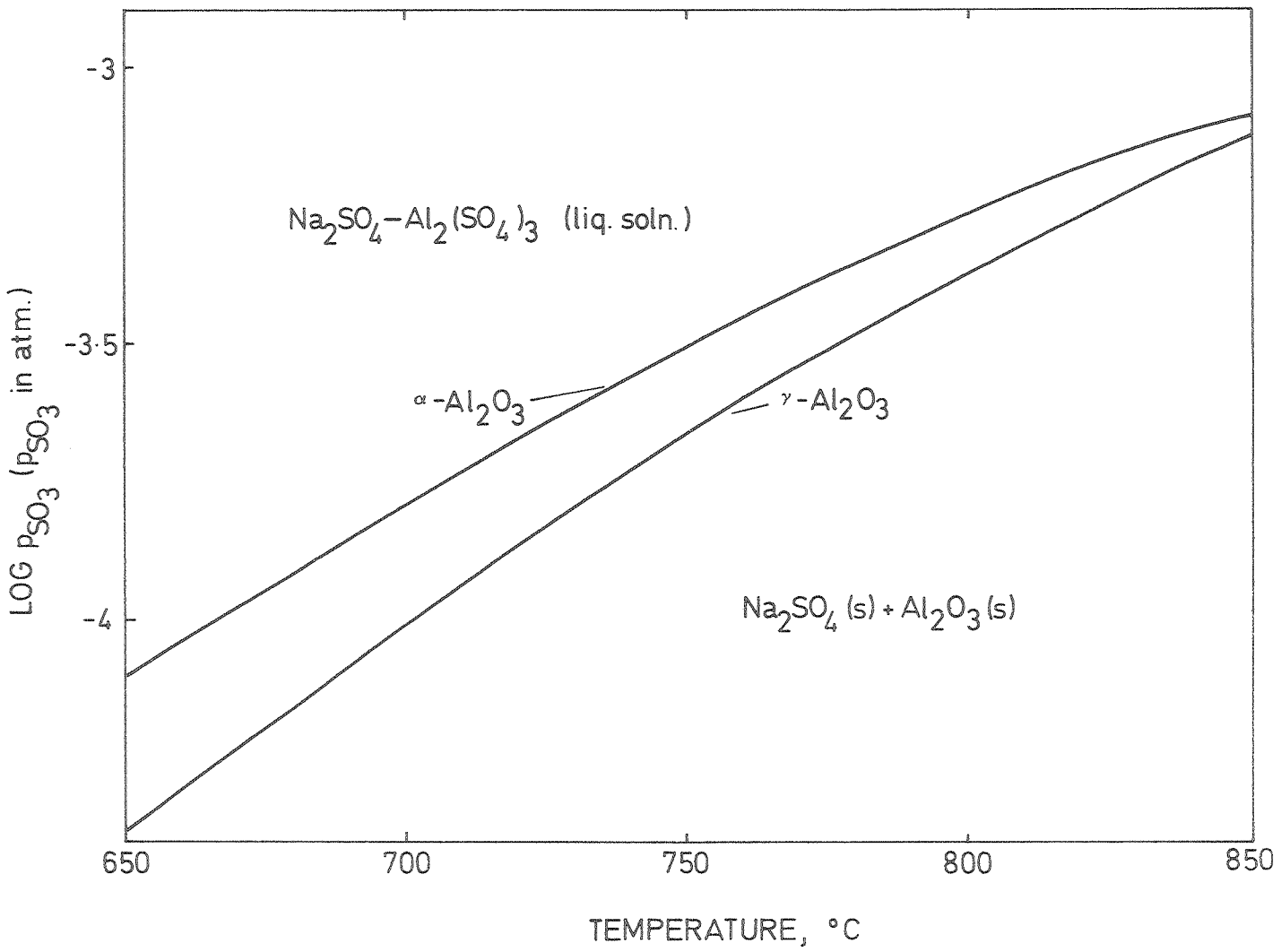

Figure 12

XBL 809-11570

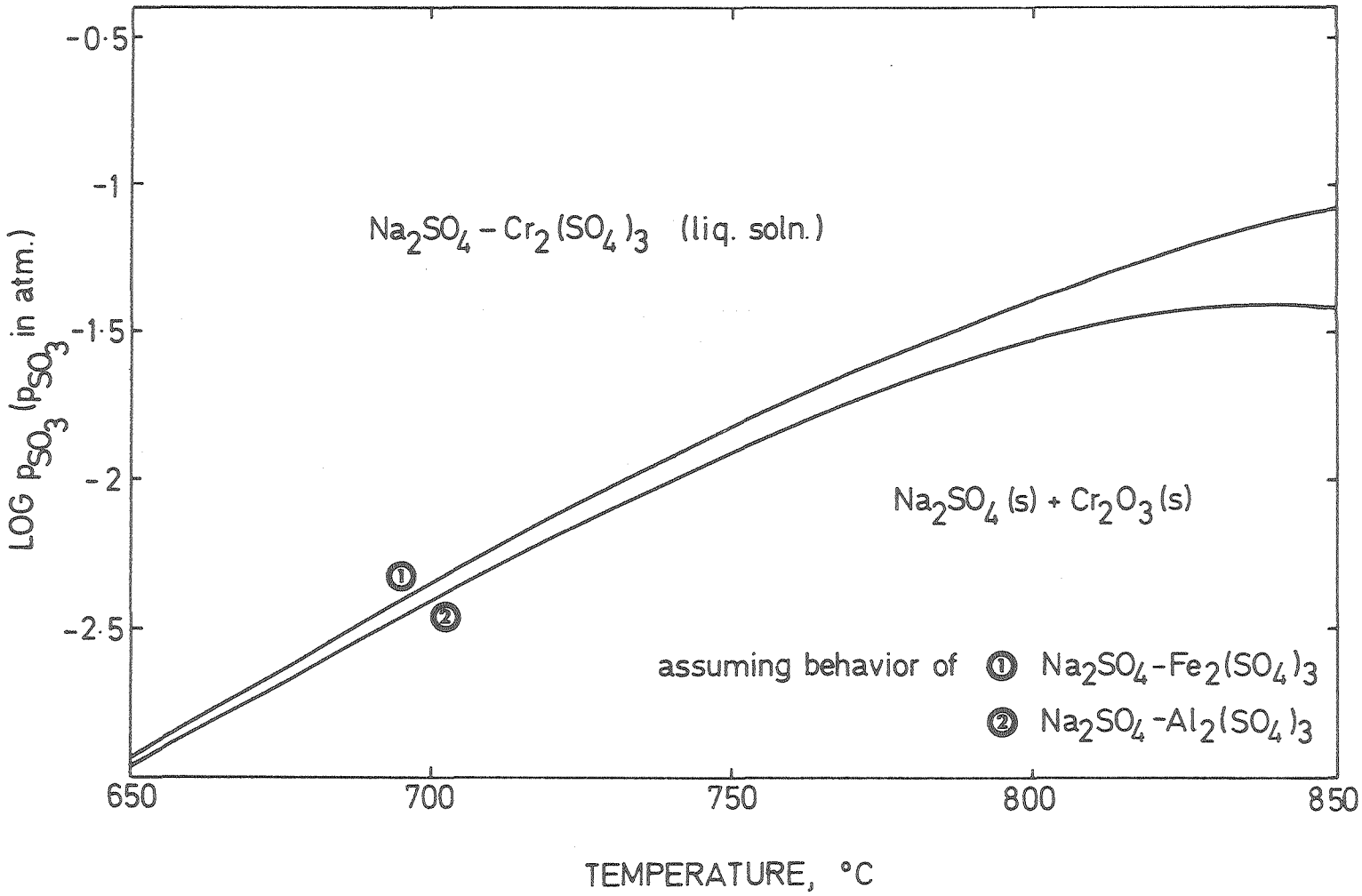

Figure 13

XBL 809-11571

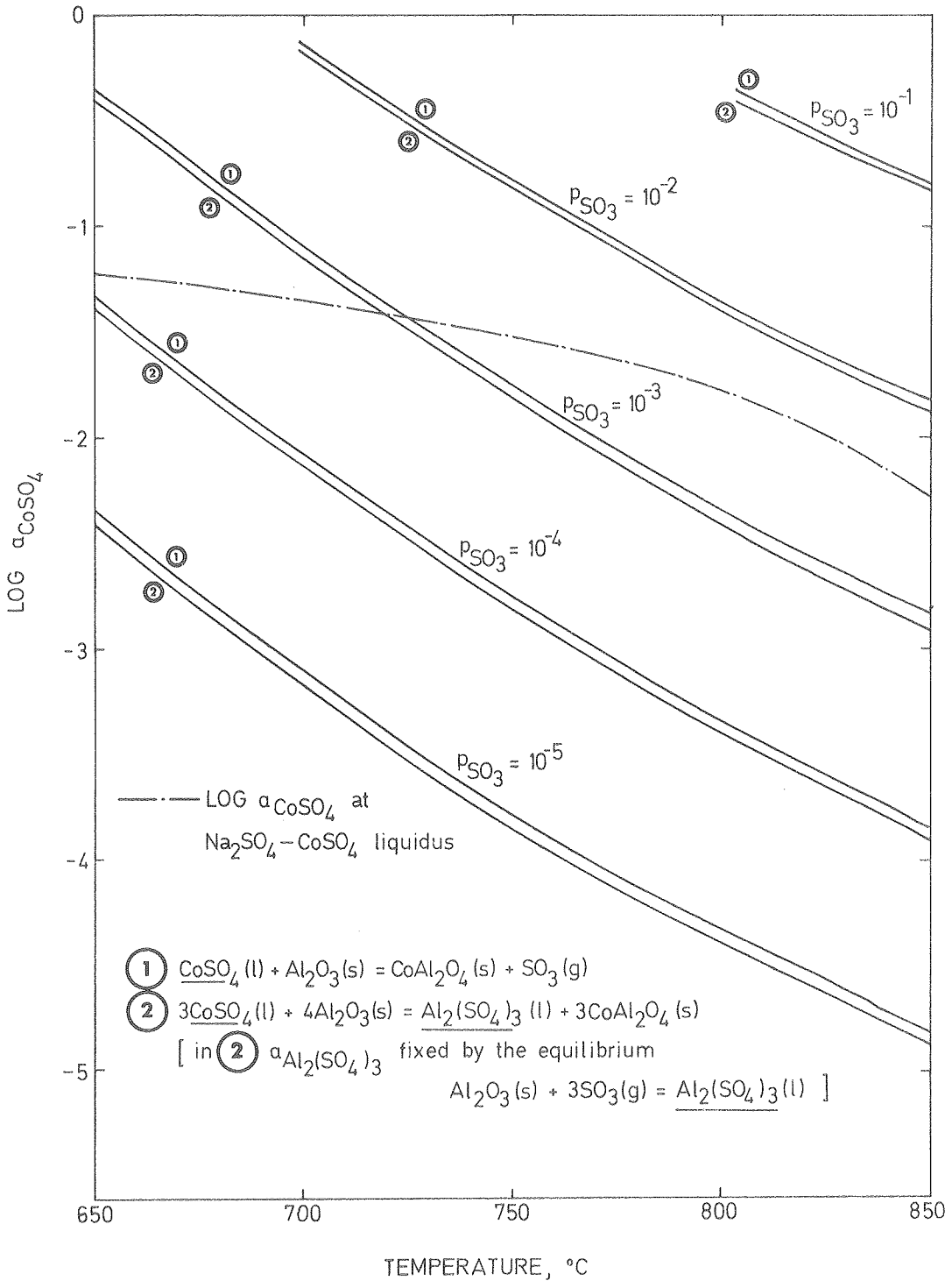

XBL 809-11580

Figure 14

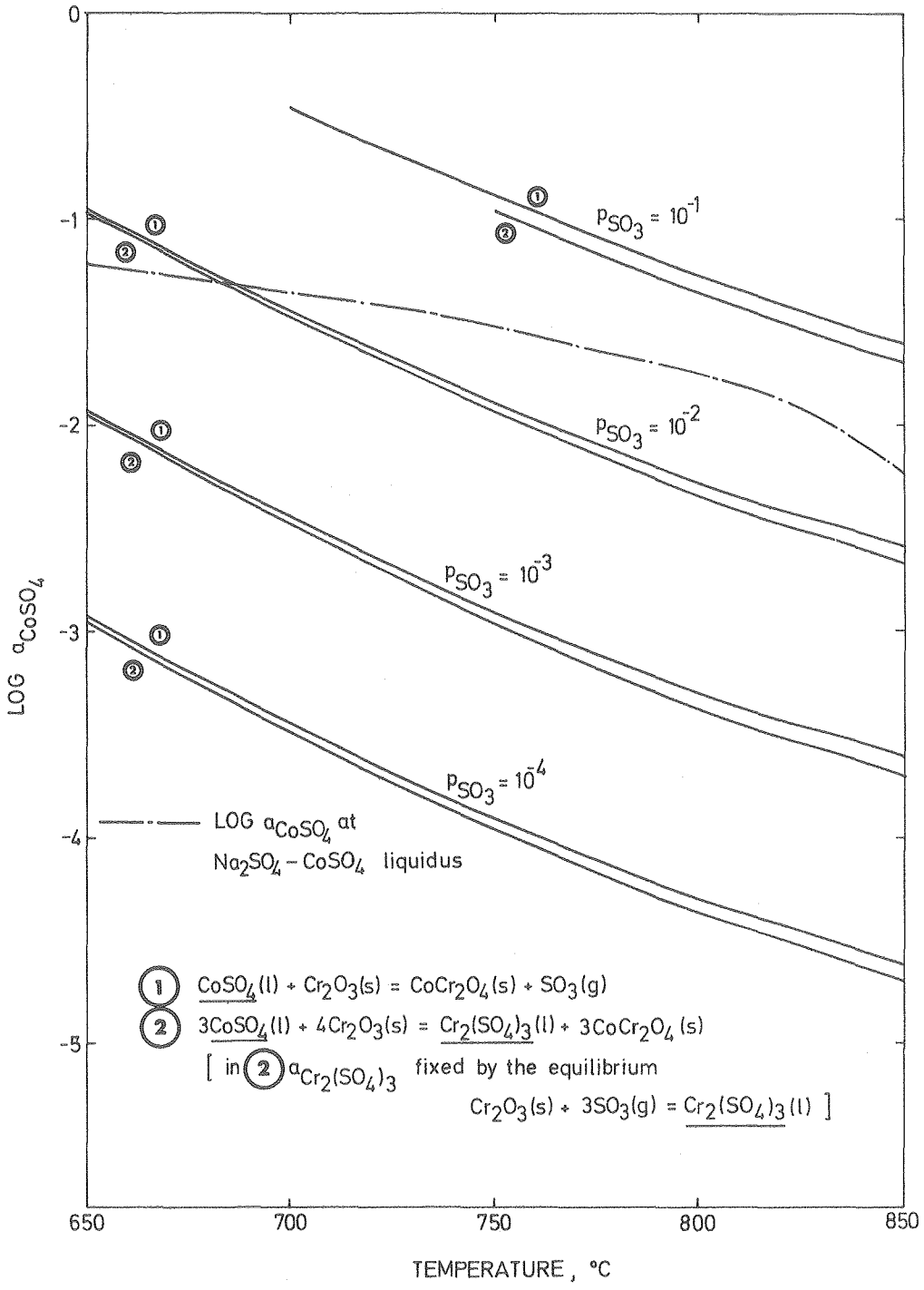

Figure 15

XBL 809-11577

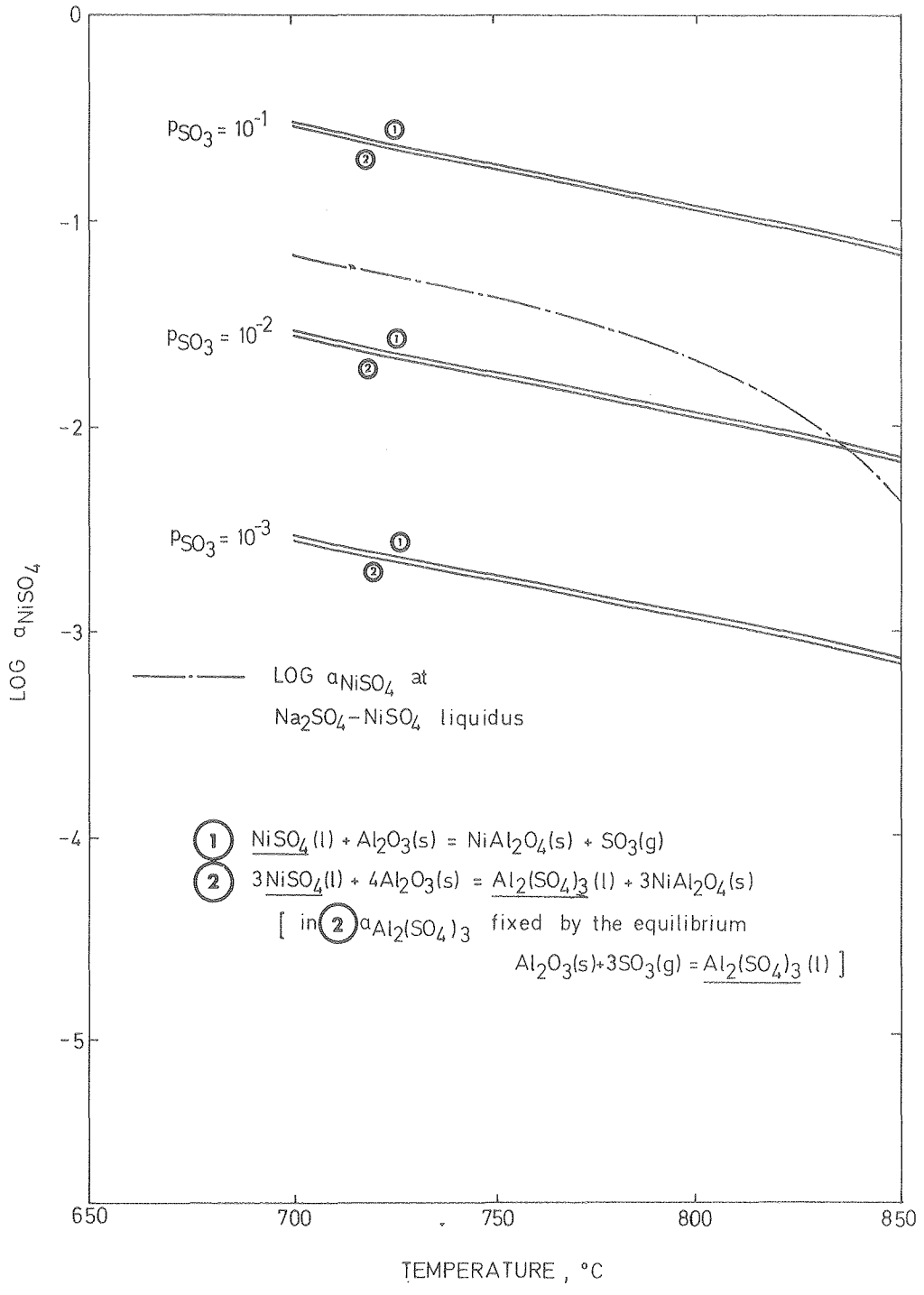

Figure 16

XBL 809-11581

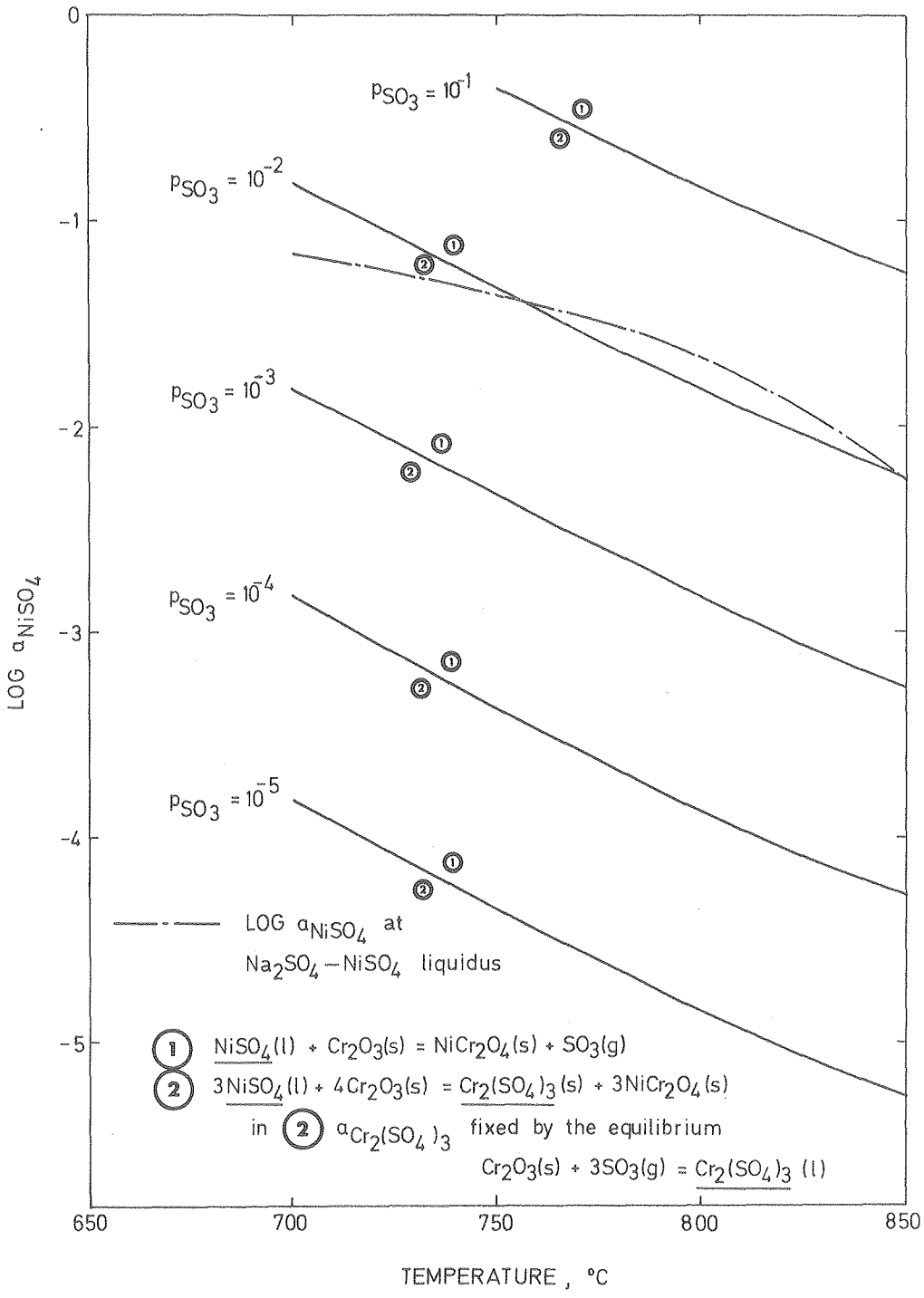

Figure 17

XBL 809-11578

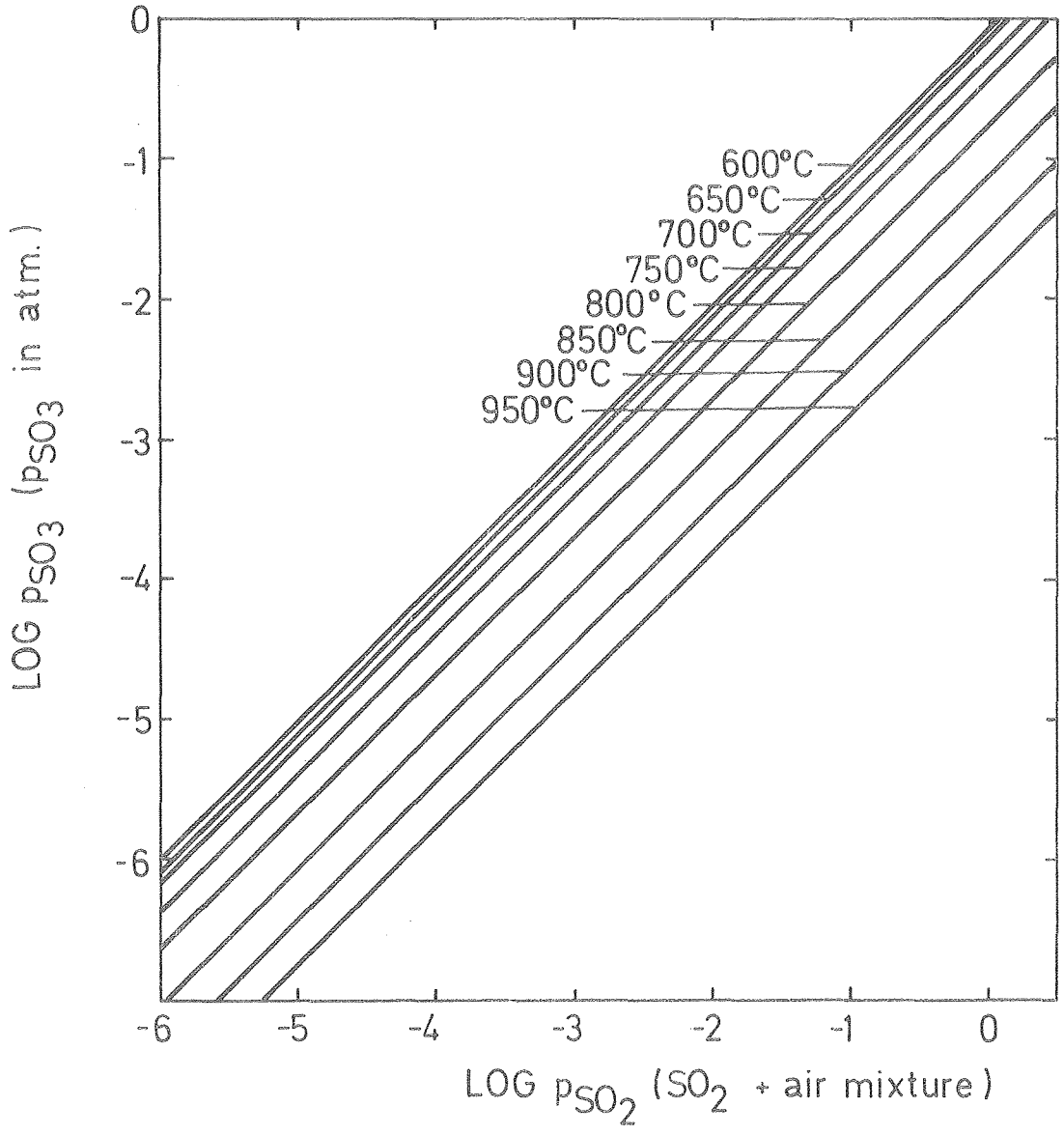

XBL 809-11575

Figure 18